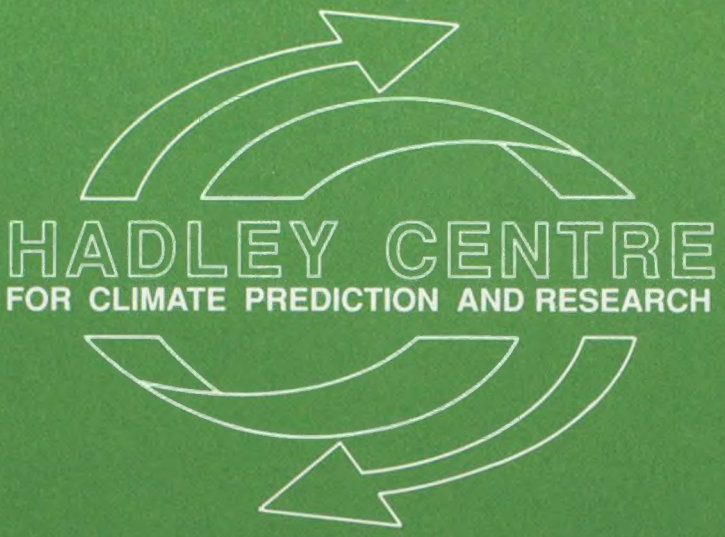

Simulation of El-Niño/Southern Oscillation like variability in a global AOGCM and its response to CO_2 increase

by

S F B Tett

CRTN 45

March 1994

CLIMATE
RESEARCH
TECHNICAL
NOTE

Hadley Centre
Meteorological Office
London Road
Bracknell
Berkshire RG12 2SY

CLIMATE RESEARCH TECHNICAL NOTE NO. 45

SIMULATION OF EL-NIÑO/SOUTHERN OSCILLATION LIKE VARIABILITY IN A GLOBAL AOGCM AND ITS RESPONSE TO CO_2 INCREASE

by

S F B Tett

March 1994

This paper has been submitted for publication in the Journal of Climate

Hadley Centre for Climate Prediction and Research
Meteorological Office
London Road
Bracknell
Berkshire RG12 2SY

NOTE: This paper has not been published. Permission to quote from it should be obtained from the Director of the Hadley Centre.

Abstract

A 75 year integration of a coupled atmosphere/ocean model is examined for tropical interannual variability. The atmospheric model has interactive cloud and a seasonal cycle. The fluxes of heat and salinity into the ocean component of the model are flux corrected. The model has tropical variability which is qualitatively similar to that of the observed El Niño/Southern Oscillation (ENSO). The maximum amplitude of the model Nino3 signal is approximately half that of the observed coupled system and the modelled ENSO time scale is greater than that observed. In the first 50 years of the integration the model has 8 warm events. Each event is one of two types: one characterized by a standing SST anomaly in the central and eastern Pacific and the other by a westward propagating sea surface temperature anomaly. The majority of the model warm events are of the first type.

The first type of event is triggered by the eastwards propagation of Kelvin waves across the Pacific and the second by westwards propagation of warm temperature anomalies through the atmospheric response to a warm anomaly causing the suppression of equatorial upwelling. There is a coupling to the seasonal cycle for the first type of event. A positive feedback through changes in marine stratocumulus in the east Pacific is an important factor in some simulated warm events.

Another integration was carried out in which atmospheric CO_2 was increased at a rate of 1% (compounded) per annum. There is no significant change in the one to ten year interannual variance of SST and this suggests that the size of the SST anomalies during warm or cold events in the "greenhouse" world may not be significantly different from those of today.

1 Introduction

One of the more important sources of interannual climate variability in the tropics is the El-Niño/Southern Oscillation (ENSO) which is a phenomenon involving both the tropical ocean and tropical atmosphere. Pioneering work by Walker and Bliss (1930) identified the periodic movement of atmospheric mass from the tropical Pacific to the tropical Indian Ocean sectors and *vice versa* and termed this the Southern Oscillation. Bjerknes (1966; 1969) showed that there was a connection between the eastern Pacific being warmer than average (El-Niño or warm events) and the phase of the Southern Oscillation. The first numerical model confirmation of this result was by Rowntree (1972). ENSO is believed by most authors to be due to the interactions between the atmosphere and the ocean. Peak warm phases of the El-Niño/Southern Oscillation are associated with changes in the tropical climate, amongst others, drought in Australia and rain in the coastal areas of Peru (Glantz *et al*, 1991).

Many models have been used in an attempt to understand ENSO and to make predictions of its phase. These models have included atmosphere only models which are forced with observed sea surface temperatures (SSTs) (Barnett *et al*, 1991), tropical ocean only models forced with observed values of wind stress (Philander and Seigel, 1985; Barnett *et al*, 1991), and simple coupled models (Zebiak, 1986; Lau, 1981; Zebiak and Cane, 1987). In recent years as available computing power has increased more complex coupled atmosphere/ocean general circulation models (AOGCMs) have been developed. Many of these coupled general circulation models have used an ocean model restricted to the tropics and a global atmospheric model (TOGA). Several of the TOGA and global ocean AOGCMs have oscillations which are qualitatively similar to that of the observed ENSO. (See amongst others Meehl (1990); Sperber and Hameed (1991); Latif *et al* (1993); Nagai *et al* (1992); Lau *et al* (1992); Philander *et al* (1992).) The characteristics and presence of tropical coupled oscillations differs between models. Neelin *et al* (1992) summarized the differing behaviour of many models.

The aims of this paper are: (1) to describe the ENSO like tropical variability in a global coupled model developed at the U.K. Meteorological Office (UKMO); (2) to compare this variability with the observed ENSO phenomenon, drawing attention to their differences and similarities; (3) to propose mechanisms for the model oscillations; and (4) to examine changes, if any, to the model ENSO in a transient experiment in which atmospheric CO_2 increased at a rate of 1% (compounded) per year.

In the next section the model is described and its climatology compared with observations. In section 3 we compare the model data with some observed statistics. In that section we also examine the tropical response during warm and cold events and again compare these with observations. In section 4 we look at two model warm events in detail so that we can establish mechanisms for the behaviour of the model. We consider the effects of increasing atmospheric CO_2 on the model interannual variability in section 5. The final section summarizes the results and draws some conclusions.

2 The Model

The model results described are from an experiment to predict the transient climate response to an increase in atmospheric CO_2 carried out at the U.K. Meteorological Office. Two integrations were carried out; a control experiment in which CO_2 was held constant at 323 parts per million and a transient experiment in which atmospheric CO_2 was increased at a rate of 1% per year (compounded). Both these experiments were integrated for 75 years from the same initial conditions obtained from a "spin-up" integration of 150 years. The model uses a flux-correction technique similar to that described by Manabe *et al* (1991) in order to keep the climate of the control experiment close to that of the observed climate. These corrections were generated from the "spin-up" part of the integration, are functions of position and time of year and do not vary interannually. For greater detail on the experiment design, model and results see Murphy (1994) and Murphy and Mitchell (1994). The comparison of the model climatology with the observed climatology as well as the understanding of the model mechanisms are all based on the results of the control experiment. The results of the transient experiment are used to draw some tentative conclusions about changes to ENSO in a warmer climate.

(a) Model Description

Both atmosphere and ocean models are global grid-point models with a resolution of 2.5° in latitude and 3.75° in longitude.

The atmospheric model is a primitive equation sigma co-ordinate model, has 11 vertical levels and a realistic orography. The model dynamic formulation and level distribution is described by Slingo and Pearson (1987). The model parametrizes gravity wave drag (Palmer *et al*, 1986), layer clouds (Smith, 1990) and convection (Gregory and Rowntree, 1990). The layer cloud scheme used is the "CW" scheme of Senior and Mitchell (1993) which uses an explicit cloud liquid water prognostic variable. They describe the performance of the atmosphere model in simulating the observed climate using that and other cloud schemes and its sensitivity to a doubling of atmospheric CO_2 for each of them. The radiation scheme used is that employed by Slingo *et al* (1988). The boundary layer scheme is also that used by Slingo *et al* (1988) with modifications to take account of cloud water (Smith, 1990). The surface and boundary layer exchange schemes are stability dependent. The behaviour of the boundary layer scheme over sea is described by Gordon (1989) where the effect of sub-grid scale "gustiness" is accounted for. Over land, evaporation and other surface fluxes are determined from parametrizations (Warrilow *et al*, 1986) which take account of the influence of vegetation, and soil characteristics, specified as spatially varying values (Wilson and Henderson-Sellers, 1985).

The ocean model is based on that of Cox (1984) and has a realistic topography and 17 unequally spaced levels. The depth and thickness of these layers are shown in table 1. The ocean is kept statically stable by the use of a convective adjustment scheme. If the vertical gradient of potential density between two vertically adjacent grid cells is unstable then the grid cell values of temperature and salinity values are mixed. Density values are obtained from the equation of state using the prescription of Bryan and Cox (1972). A mixed layer model, based on that of Kraus and Turner (1967) is embedded in the ocean model. The sea ice model is based on that of Semtner (1976) and the performance of this component of the model is discussed in Roberts and Cattle (1989). The low resolution of the ocean model necessitates a horizontal

Table 1: Ocean model level depths (m)

Model Layer	Thickness	Depth of mid-point
1	10.0	5.0
2	10.0	15.0
3	10.0	25.0
4	10.2	35.0
5	15.3	47.4
6	23.0	66.5
7	34.5	95.8
8	51.8	138.9
9	77.8	203.7
10	116.8	301.0
11	175.3	447.1
12	263.2	665.3
13	395.3	995.6
14	593.5	1490.0
15	891.1	2232.3
16	1236.2	3295.9
17	1586.0	4707.0

eddy viscosity coefficient of 3×10^9 cm^2/s. Furthermore there is a small amount of diffusion carried out along isopycnal surfaces using the formulation of Redi (1982). The mixing coefficient for this diffusion varies exponentially with depth decreasing from $2 \times 10^7 cm^2/s$ at the surface to $1 \times 10^7 cm^2/s$ at a depth of approximately 500 metres. Vertical mixing, in addition to cross isopycnal mixing, uses the scheme of Pacanowski and Philander (1981). The coefficients of diffusion and viscosity vary from a background value of $0.1 cm^2/s$ to a maximum value of 55 cm^2/s. Throughout the ocean mixed layer the vertical diffusion is at its maximum value of 55 cm^2/s.

The only driving terms for the model are the incoming short wave radiation fluxes which have a seasonal cycle.

As discussed earlier the model uses a flux-correction technique to keep the model climate close to that observed. The terms corrected are those for heat and salinity. Fig. 1 shows the annual means of the heat and fresh water flux corrections in the tropical region. Note the positive correction in the heat flux along the Pacific equatorial region. There is also a small region of strong negative heat flux correction off the west coast of South America. The fresh water flux corrections have a large region between 180° and 150°E on the equator of positive fresh water flux in excess of 5 mm/day. In addition there is a smaller region over Indonesia with fresh water fluxes greater then 5 mm/day.

(b) Model tropical climatology

In this subsection various parts of the model climatology are presented and where possible these results are compared with observations. The model has a climate drift in the Southern Ocean and possible reasons for this drift are discussed in Murphy (1994). This drift causes the Southern Ocean to heat up and eventually this heating propagates northwards into the equatorial region. Prior to year 50 this drift does not influence the tropical region. Therefore a climatology for the tropics is constructed using years 1 to 50 of the model integration.

The SST, subsurface ocean structure, surface stresses, outgoing longwave radiation and albedo are examined. Fig. 2 shows the June, July August (JJA) mean and the December, January, February (DHF) mean SST fields from the model and observations. The observations of sea surface temperature are from the Global Ice and Sea Surface Temperature (GISST) data

set of the U.K. Meteorological Office (Parker *et al*, 1993). This data-set is a development of a previous U.K. Met. Office global sea surface temperature data set described in the atlas by Bottomley *et al* (1990). The model climatology is for years 1 to 50 of the integration while the observed climatology is for the period 1948 to 1988. The model and observed climatology of sea surface temperature have very similar fields as would be expected given the flux corrections. The major difference between the two is that the model JJA climatology has the cold tongue extending slightly further west along the equator compared to the observed climatology. In addition the region where the temperature is greater than 29°C is smaller in the model than observed. In DJF the differences are small; the warm water off the west coast of central America is less extensive in the model compared to the observations and the model is slightly cooler to the east off Brazil. The location and sizes of the warm pools and cold tongues are similar to that observed.

We now consider the model surface wind stress fields and compare them to the mean observational wind stresses of Hellerman and Rosenstein (1983). These observed wind stresses are normally multiplied by 0.75 when used to drive tropical ocean models (Stockdale *et al*, 1993) and this is also done here when comparing the observed wind stresses with the model wind stresses. Fig. 3 shows the model climatology of wind stress for JJA and DJF. The magnitude of the model wind stress is close to that of the observed wind stress. The simulated climatology of wind stress magnitude in the tropics has slightly higher values. (JJA mean magnitude tropical model value: 0.06N/m^2, JJA mean magnitude tropical observational value: 0.058N/m^2, with the corresponding values for DJF being 0.057 and 0.051 respectively). The model succeeds in representing the seasonal reversal of the wind stress in the west Indian Ocean. Large scale convergence of the trade winds into the equatorial region is also reasonably well modelled. There are some differences in the JJA wind stresses; the model has a region of northeastwards wind stress to the east of the Philippines which is not present in the observations. The model also displaces the southeast trades, particularly near the South American coast, to the north and east of their observed positions in both JJA and DJF and slightly strengthens them relative to the observed values. The model does not represent the strength of the southwesterly winds in the Arabian Sea during JJA. Furthermore off the west coast of Central America the model has westerlies that are too strong. During DJF the model strengthens the northeast Pacific trades off Central America. In the northern Indian Ocean the modelled wind stresses are too high compared with those of Hellerman and Rosenstein (1983).

Fig. 4 shows zonal cross sections of annual mean temperature and all components of ocean velocity along the equator. Fig. 5 shows meridional cross sections for the annual mean temperature and velocity components at 150°W. In both figures the components of velocity parallel to the plane have been shown as arrow plots overlaying the temperature contour plot while the perpendicular component has been shown in a separate contour plot. The vertical velocity component has been considerably exaggerated.

The model simulations of ocean temperature and currents can be compared to the atlas of Levitus (1982), the results of the Hawaii-Tahiti shuttle experiment (Wyrtki and Kilonsky, 1984) and the estimated values of equatorial upwelling made by Halpern *et al* (1989). In general model currents are significantly weaker than observed, particularly below a depth of 50 metres. Compared with Fig. 2 of Wyrtki and Kilonsky (1984) the plot of simulated zonal current at 150°W shows an extremely weak under current (peak value of 0.1 m/s compared to a peak observed value of 0.9 m/s). The model fails to simulate the north equatorial counter current though it does simulate the main equatorial current with approximately half the magnitude and with peak values of the current being closer to the surface than observed. Mean simulated vertical velocities at 50 metres are about half those estimated in the equatorial Pacific by Halpern *et al* (1989) (1.3×10^{-6} m/s compared to 2×10^{-6} m/s) but while estimated Pacific vertical velocity values are greater than 2×10^{-6} m/s at 150 metres the modeled values are 0.2×10^{-6} m/s at that depth.

Throughout the entire equatorial region the simulated vertical temperature gradient is weaker than observed though the shoaling of isotherms in the eastern Pacific is represented in the model.

The model does have some equatorial asymmetry in the temperature field as does the observed temperature cross section. The directly wind driven equatorial currents are broader than observed and have magnitudes about half that observed. The under current, being density driven, is much weaker than observed perhaps because the large amount of diffusion of temperature and ocean currents required for numerical stability will reduce the ocean pressure gradients and thus the magnitude of the pressure gradient driven currents.

We next wish to compare the model cloudiness with observed clouds. Direct comparison between model clouds and satellite derived clouds is a difficult task – we can not be sure we are comparing the same thing. However we can look at the effects of clouds *via* the radiation budget at the top of the atmosphere.

Therefore we now compare the shortwave albedo and top of the atmosphere outgoing longwave radiation (OLR) fields from the model with the same quantities from the ERBE dataset (Harrisson *et al*, 1990). Fig. 6 shows model climatology plots of albedo for January and July for the years 1 to 50. Also shown in that plot are the differences between the model and the ERBE climatology for the period 1985 to 1989. Fig. 7 shows similar plots for the OLR fields. We interpret these figures in the following way; over the oceans high values of albedo and high values of OLR correspond to low level cloud such as the marine stratocumulus decks to the west of the continents; low values of OLR and high values of albedo occur in regions of high cloud associated with deep convection. Comparison, not shown, of OLR and albedo values with model values of cloud support this interpretation.

In January (figures 6(a), (b) and 7(a), (b)) insufficient low cloud is being generated off the west coast of South America by the model from 10°S southwards. During January the model generates too much high cloud over the west Indian Ocean and off the west coast of central America but not enough high cloud over the Indonesian and east Indian Ocean regions. In both the South Pacific and South Atlantic Convergence Zones regions the model has lower values of OLR than observed suggesting that there is more simulated high cloud than occurs in reality.

In July (figures 6(c), (d) and 7(c), (d)) the modelled low level cloud off the west coast of South America is displaced to the north and west of its observed positions. The northwest tropical Pacific has lower OLR and higher albedos than the ERBE observations suggesting that too much high cloud is being generated in this region in particular along the oceanic ITCZ. The model simulated Indian Monsoonal high cloud is displaced to the south and west of India. Throughout the entire tropics the oceanic ITCZ has lower than observed values of OLR suggesting too much cloud is present in these regions in the model. Over the major centres of convective activity, that is the maritime continent, South America and west Africa, OLR values are greater than observed.

Means of OLR over the tropics compare well with the observations. The model's mean values are approximately 5 Wm^{-2} greater than the observed values in both January and July. The mean albedo values also correspond well with the model having values of 24.8% for January and 25.1% for July compared to the ERBE values of 24.1% and 24.7% for the same months.

Other parts of the annual cycle, not shown, have a broadly similar picture with an insufficient amount of marine stratocumulus cloud and a displacement of that cloud away from the coasts. The OLR values in Indonesia, Africa and South America are greater then the observed values while over the oceanic convergence zones modelled OLR values are less then the ERBE observations.

In summary the simulated SST compares well with that observed, model wind stresses are slightly stronger in the Pacific than observed and the southeast trade winds in the east Pacific are displaced to the north and east of their observed positions. Over the oceans the model does not generate sufficiently large regions of low shortwave albedo. The model also has the marine stratocumulus off the coast of South America displaced to the west by about 10° of latitude. Furthermore in the centres of convective activity the model has smaller values of OLR than observed, suggesting that more high cloud than observed is present. However in the oceanic convergence zones the model has smaller values of OLR than observed. The model ocean thermocline is too diffuse and the currents are weaker by between a factor of two and ten

compared with those observed with the closest agreements to the observed estimates occurring near the surface.

3 Model ENSO

In this section the behaviour of the model ENSO-like oscillation will be examined. We will do this by first considering the timeseries of SST in the east Pacific and of pressure differences across the Pacific. Time-longitude plots of equatorial SST using seasonal data from the model will then be compared with a similar plot using observed data. An EOF analysis will show that changes in pressure are highly correlated with those of SST. We will then look at modelled changes in the tropics for all warm and cold events. These changes will then be compared with the observed changes. Finally a composite difference between all warm and cold events will be examined.

(a) Oscillations

We first show that the model has an oscillation that involves both the ocean and the atmosphere. Fig. 8 shows the SST seasonal anomaly signal for the Nino3 region (150°W,10°S to 90°W,10°N)) in the east-central Pacific. Also shown is the seasonal anomaly pressure difference between the model grid-points nearest to Tahiti (150°W, 18°S) and Darwin, Australia (128°E, 12°S), that is the southern oscillation index (SOI). For both timeseries the anomalies are relative to the seasonal means for years 1 to 50 of the model integration. The model Nino3 signal is weaker than observed, with a peak value of 1°C compared to an observed peak value of 3°C. The model SOI signal is also weaker than observed.

Notice how strong positive SST anomalies are correlated with strong negative pressure difference anomalies. The two anomalies have a correlation of -0.55 whereas the 3 season smoothed values have a correlation of -0.69 suggesting that over longer timescales the Nino3 and SOI indices are well correlated. The climate drift that occurs approximately after year 50 of the integration can also be seen. Also shown in Fig. 8 are the power spectra from years 0 to 50 of the model integration. The model Nino3 signal has a considerable amount of power in the long period (greater than 100 months) but only 3 to 4 cycles for that period are available in the 50 year data set. Of more relevance to this paper is the variability in the period range 25 to 80 months. There are several peaks here in the SST spectra but two between approximately 50 months and 70 months have peaks coincident with those of the SOI signal. The observed spectra of SST data for the period 1953–1974 exhibits maxima in the 3-5 year time scale (see Fig. 6 of Rasmusson and Carpenter (1982)).

Fig. 9 shows longitude/time plots of the sea surface temperature, for the equatorial region (2.5°N to 2.5°S), from the first 30 years of the model integration. This figure shows that the model has interannual variability with, for example, a relatively strong warm event in year 17; the region of temperatures above 29°C having moved eastwards to cross the dateline. Cold events can be seen at the end of years 2 and 30 with the regions of warm water having moved further to the west. Interdecadal variability can be seen in this plot. The reasons for this are not known. However when an atmospheric model was coupled to a simple ocean mixed layer model Barnett *et al* (1992) found that the coupled model had long period variability in the tropics.

Fig. 10 shows a similar plot for the observed SSTs from the GISST data-set for the 30 year period from 1960 to 1990. There are also some similarities in both plots with warm water moving eastwards during the observed strong warm events such as 1982 and 1987 and warm water moving westwards during observed cold events such as 1988. There are some qualitative differences between the two figures; on several occasions the observed data has a coherent region with temperatures greater then 29°C spanning the Indian Ocean while only on a few occasions does the model have such a feature. The model is also more active in the east Indian Ocean than is observed with several occasions in which temperatures are less than 28°C. Compare this to the observed record in which there is only one year (1962) in which temperatures in the east Indian Ocean are less than 28°C.

We now examine the largest modes of variability in both the model and observations using empirical orthogonal functions (EOFs). We examine EOFs from the tropical region for both model and observations in order to compare the major modes of variability using the area weighted covariance matrix. We use SST and sea level pressure data with the mean annual cycle removed, as we are looking at the anomaly variability patterns over the entire annual cycle. The observed data is from the period 1960 to 1988 with the pressure data being taken from the COADS data-set with corrections as made by Ward (1992) while the temperature data-set is the U.K. Met. Office GISST data-set referred to earlier. This period is chosen because the pressure data prior to 1960 has large regions of missing data. Fig. 11 shows the first EOFs of these data-sets. The same missing data masks were used for model and observed pressure data sets. The observational pressure data are on a $10^\circ \times 10^\circ$ grid and the model pressure data were interpolated onto this grid prior to the computations being carried out.

The two SST EOFs (plots (a) and (b)) are qualitatively similar, both having a large signal in the equatorial east Pacific. Both EOFs have been scaled so that they have positive weights in the east Pacific and are orthonormal. As well as qualitative similarities between the two EOFs there are also several differences. The model SST EOF does not have such a strong well defined maximum as do the observations, neither do the observations have a signal in the northeast tropical Pacific which is present in the model. The model has a stronger region of opposite sign in the west Pacific to the east Pacific signal than do the observations. Note that the time coefficients of both the first SST EOFs correlate significantly with the time series of mean temperature in the Nino3 region (0.95 for the observed data and 0.78 for the simulation).

Both the model and the observed pressure EOFs are have strong weights over the Indonesian region. However the model EOF has weaker weights than observed in the east Pacific and has almost no signal over the Atlantic Ocean. The timeseries for the first pressure EOFs are highly correlated with that of the first SST EOFs (0.89 for observed data and 0.86 for model data). The high correlations between the first model EOFs of pressure and SST suggest that processes similar to those occurring in the natural ENSO cycle could be happening in that the model cycle involves correlated changes in both the ocean (SST EOF) and in the atmosphere (pressure EOF).

The percentage of the variance explained by the model EOFs is lower than that observed with the model EOFs explaining about 20% of the variance compared to about 30–35% of the variance for the observed EOFs. As the magnitude of the model ENSO is weaker than that observed, this does not seem particularly surprising, since other, non ENSO, physical phenomenon will contribute relatively greater amounts of variance in the model compared to that of reality.

(b) Response

In this subsection we examine meridional means of the tropics during model warm and cold events and compare these to observations in order to examine the model states during warm and cold events. We also examine the atmospheric response of the difference between a DJF warm event composite and a DJF cold event composite.

In order to examine the model response we require a definition of a warm event and of a cold event. We define a warm event as follows. When the standardized Nino3 anomaly (SST seasonal anomaly for the Nino3 region divided by the standard deviation for that season) is greater than 0.5 and the standardized SOI is less than -0.5 , then the year is a warm event year. The season DJF is assigned to the year in which December falls. That is DJF of year N is taken to be an average over the period starting in December of year N and ending at the end of February of year $N+1$. This definition when applied to the observational record, for the period 1948 to 1990, gives the following warm events: 1951, 1953, 1957, 1963, 1965–1966, 1968–1969, 1972, 1977, 1982 and 1986–1987. During the first 50 years of the control integration the model has warm events, using the same definition, in years 1,4, 10, 16–18, 21, 38, 43-44 and 47. We now examine the mean tropical response for these years. We do this by looking at meridional means of anomalies relative to the years 1 to 50 climatology from each event, in the region between 10°N and 10°S during DJF of the years identified above. When events last two years, the first year DJF is

examined. When they last three years the second year DJF is examined. The variables that we consider are sea level pressure, precipitation, the zonal component of wind and the sea surface temperature.

Fig. 12 shows those quantities for all eight warm event years. In all the events the SST is reduced in the west Pacific and increased in the east Pacific though the strength and detailed position varies between events, the largest temperature rise in five of the events being off the west coast of south America. In five of the events (year 1, 4, 10, 17 and 43) the Atlantic sector also shows some warming. The mean sea level pressure signal has higher pressure over the west Pacific and lower pressure over the east Pacific, in all but the year 47 event, than does the seasonal norm. There is a shifting east of the precipitation which is shown by an increase in precipitation between 120°E and the dateline and a fall in precipitation between 60°E and 120°E. There is also a reduction in precipitation in all but the year 43 event over South America. The response in the zonal wind is consistent with the convective region moving further east. Regions of reduced precipitation have reduced convergence and regions with increased convergence have increased precipitation.

There is considerable variability in the details of the atmospheric response between warm events. For example the model year 17 event is extremely strong while the year 47 event is very weak. However in nature there is no "canonical" El-Niño; events differ from one another. Note that six model warm events occur in the first 21 years and after that there is not another event for 17 years. The model has a large amount of variability in the long period end of the spectrum and during this 17 year period the model is cooler than average.

A cold event is defined symmetrically to a warm event, that is standardised Nino3 temperature < -0.5 and standardised SOI > 0.5. This definition gives, for the observational record, the following years as cold events; 1949–1950, 1954–1956, 1961–1962, 1964, 1970–1971, 1973–1975, and 1988–1989 and for the model integration the following years; 2–3, 5, 8, 29–30, 36–37, 40–41, 45 and 49.

Fig. 13 shows a similar plot to Fig. 12 but for the cold events listed above. The general picture that this figure gives, is of cooler temperatures in the east Pacific and warmer temperatures in the west Pacific/east Indian Ocean. In four of the cold events (year 2, 5,8 and 40) the Atlantic is cooler than normal. Sea level pressure tends to decrease in the west Pacific and to increase in the east Pacific. Precipitation tends to increase in the west Pacific/east Indian Ocean (at about 120°E) and decrease slightly across the east Pacific. The changes in wind are consistent with enhanced convergence into regions of increased precipitation. In general the signal from the model cold events is the opposite of the model warm events in the Pacific and Indian Ocean regions; the model is behaving similarly to observations in this respect as observed cold events are also the opposite of observed warm events.

How do modelled warm events compare with real warm events ? Fig. 14 shows plots for DJF of the year of the 8 observed warm events since 1957. The SST data is from the GISST dataset, the wind and pressure data are from the COADS dataset with corrections as made by Ward (1992) and the precipitation data are from the CRU rainfall dataset extended to 1990 (Hulme, 1992), though note that these data are for land stations only. The COADS data contains several areas of missing data. Both the model and the observations show an increase in temperature in the east Pacific though in the observations the anomalously warm temperatures occur east of the dateline and in the model the warm anomalies are to the east of 160°W. In the east Indian Ocean/Indonesian region the model is cooler than normal. There is also a tendency for the observed temperature to show some cooling centred on 150°E. This cooling is stronger in the model, too far to the west and much broader in extent than that observed. Associated with these changes in surface temperature are changes in sea level pressure. Pressure anomalies in the simulated west Pacific are always positive but whereas in the east Pacific the observations always show negative anomalies some model events show weak positive anomalies. Precipitation changes are larger in the model than in nature and tend to happen further east than in real warm events.

As pointed out earlier the model fails to simulate an adequate Indian monsoon, with the

enhanced convective activity occurring over the Indian Ocean rather than over the subcontinent. Nevertheless during cold events (associated with a high value of the SOI) there is enhanced rainfall in the east Indian Ocean sector during northern summer. Ropelewski and Halpert (1987) showed that there is greater than normal precipitation during the Indian Monsoon in 15 out of 18 observed cold events in the period 1885–1983. During cold events the model warm pool and convective region are displaced to the west. During warm events the warm pool and convective region move eastwards. Given these movements, one might expect enhanced rainfall to the east during a warm event and enhanced rainfall to the west during a cold event. Ropelewski and Halpert (1987) show that for island stations in the central Pacific and south central Pacific there is enhanced rainfall during warm events. Ropelewski and Halpert (1989) report on a reduction in rainfall to the east during cold events. During the 1982/1983 and 1986/1987 warm events there was a movement eastwards of positive outgoing longwave radiation anomalies (Kousky and Leetmaa, 1989) suggesting that the convective region had moved eastwards.

We examine the differences between warm and cold events. We do this by forming composites of mean sea level pressure, surface temperature and precipitation for all 8 model warm events and all 8 cold events. Fig. 15 shows the differences between these composites for northern winter. Regions of significant differences (at the 5% level using Student's t-test) are shown with darker backgrounds in all the plots. The impact of modelled warm events on the DJF climate in the Southern Ocean is likely to have been contaminated by the model climate drift occurring in that region and therefore will not be considered.

We see that the model is warmer in the east and central equatorial Pacific and in the north-east subtropical Pacific during warm events than during cold events. In the southern tropical Pacific, north-west tropical Pacific and north-west Atlantic Ocean warm events are cooler than cold events. Other regions of significant warming are in the west Indian Ocean and northern South America. Furthermore the model has regions of warming in North Africa, Indochina and eastern Australia with some cooling occurring over the Gulf coast of the United States.

Significant pressure changes are less extensive with reduced pressure being found in the east Pacific and an increase in pressure occurring in the west Pacific and Indian Oceans. Precipitation decreases in the north of South America, Indonesia and southern Micronesia with increases taking place in parts of China, the west-central Pacific Ocean, Mexico and the north-west Pacific. For the JJA composite, not shown, the model shows no significant changes in precipitation outside the tropical Pacific region.

To summarize the model has an oscillation in the east-central Pacific region surface temperatures which has a significant correlation with the model SOI. The correlation is less than that observed. However as the magnitude of the model temperature anomalies forcing the atmosphere is smaller than that observed then the atmospheric response will also be weaker than that observed. The EOF analysis of SST and sea level pressure shows that there are some similarities between the model and observations. However, the observed SST EOF has a peak signal off the coast of South America and on the equator, while the model's maximum weights reach further west than do the observations and are less coherent than those of the observations. The model sea level pressure EOF has almost no weight in the Atlantic region. The timeseries for the first model temperature and pressures EOFs are highly correlated as are the equivalent timeseries for observed EOFs. In both model and observed warm events, the east Pacific and west Indian Oceans tend to be anomalously warm while the west Pacific/east Indian Ocean regions tend to be cooler than normal. Model cold events have essentially the opposite signal to that of model warm events. The model also has the precipitation shifted to the west (east) during cold (warm) events. This phenomenon is also observed in nature. Composite warm and cold event differences show some changes in precipitation in the tropical regions outside the Pacific.

4 Mechanisms

In this section the mechanisms responsible for the model ENSO like oscillations are explored. This is done by examining two events in detail and then generalizing to other events. There are

two different mechanisms operating in the model; one in which SST anomalies propagate westwards due to coupled atmosphere/ocean processes as proposed by Neelin (1991); and another, triggered by eastwards propagating Kelvin waves, in which the ocean surface warms almost simultaneously over the entire central and eastern Pacific as proposed by Wyrtki (1984). We now examine two events in some detail – each of which is a clear example of an event in which one type of mechanism dominates. These events are the year 10 event and the year 21 event.

(a) Kelvin wave initiated event

In this subsection we examine the year 10 event. This event has its peak phase in the early part of year 10 and is an example of an event triggered by Kelvin waves. Prior to the event a change in thermocline depth can be seen propagating eastwards across the Pacific in the form of a Kelvin wave packet. The thermocline in the east Pacific is shallow (approximately 30 metres) and changes in its depth can affect the SST in that region. Thus this propagating deepening packet causes the SST to warm. Air/sea interactions discussed in the next subsection then cause these SST anomalies to increase and propagate westwards. The thermocline depth can be measured using the vertically averaged temperature (VAT). VAT is proportional to heat content and as Rebert *et al* (1985) showed the Pacific thermocline depth near the equator is closely related to the ocean heat content and thus VAT, with large values of VAT corresponding to a deep thermocline. An increase in VAT occurs when the thermocline is deeper than normal and a reduction in VAT happens when the thermocline is shallower than normal.

Fig. 16 shows time-longitude cross sections of anomalies in the equatorial region (10°N to 10°S) for the three year period starting in January of year 8 for SST, VAT from the surface to a depth of 360 metres, and zonal wind stress. During the cold event of year 8 the sea surface temperature is warm in the west Pacific and east Indian Ocean (Fig. 16(a)). During the year the VAT anomalies grow larger in the west Pacific/east Indian Ocean region (Fig. 16(b)). However near the start of year 9 the VAT anomalies (or thermocline depth) in this region rapidly fall to values near to their normal seasonal values. The return of the thermocline to normal values has associated with it the release of an eastward propagating signal, shown by anomalously high values of VAT propagating across the Pacific. Two questions then follow from this; what causes the deepening of the thermocline and what subsequently causes the propagation of a Kelvin wave packet out from the west Pacific ?

From July till December of year 8 the waters in the Indonesian Region and to the west of it are anomalously warm. These warmer waters induce anomalously westerly wind stress as shown in Fig. 16(c), with peak values in October. This enhanced westerly wind stress then acts to deepen the thermocline shown by the anomalously high values of VAT in the Indonesian region. As the sea surface cools the anomalous zonal wind stress rapidly falls leaving the deepened thermocline out of balance with the atmospheric wind stress. The oceanic response to this is the release of an eastward propagating positive VAT anomaly.

Fig. 16(b) shows the VAT anomaly starting to propagate eastwards in about January and reaching the east Pacific coast by May. Fig. 17 shows maps of VAT and vertically averaged zonal velocity for February and April of year 9 in the tropical Pacific Ocean. Examination of these maps show that the positive VAT anomalies extend only a short distance from the equator and that they propagate westwards as do the zonal velocity anomalies. The coupled model by April (17(c)) of year 9 has a region of positive VAT to the east of New Guinea and a narrow tongue of positive VAT anomaly along the equator. Compare this with Fig. 3 of Kousky and Leetmaa (1989) which shows dynamic height anomalies for an ocean model forced with observed wind stresses for May of 1987. They also show positive height anomalies to the east of New Guinea and a narrow tongue of positive height anomalies along the equator. Cross sections of ocean temperature anomalies along the equator, not shown, have peak changes in temperature along or near the mean position of the 21° isotherm. These observations suggest that the changes in VAT are the result of wave packets propagating eastwards along the thermocline. In the equatorial wave guide only Kelvin waves can propagate eastwards and thus we conclude the propagating signals are due to Kelvin waves. In nature free Kelvin waves take 2–3 months to cross the Pacific

basin (Cane and Moore, 1981) compared to 4–5 months for the model. There is no evidence of these waves reflecting at the eastern boundary of the Pacific to form westward propagating Rossby waves as occurs in many other models (Suarez and Schopf, 1988).

The impact of the Kelvin wave signal is to deepen the thermocline, shown by the increase in VAT. This deeper thermocline allows the surface mixed layer and thus SST to warm up as the water it entrains from below will be warmer than normal. The model SST begins to warm across the entire eastern and central Pacific from May onwards though the strongest response is in the far eastern Pacific Ocean. The SST anomalies then propagate westwards stopping at approximately the date line.

To summarize; warm SST anomalies in the Indonesian region cause increased westerly wind-stress to the west of them which causes a deepening of the thermocline in the west Pacific/east Indian Ocean. As was shown in Fig. 13, cold events tend to have warmer water in this region. The termination of this enhanced wind stress due to the SST anomalies cooling causes the thermocline depth to be out of balance with the atmospheric wind stress. The ocean response to this is to cause a packet of Kelvin waves to propagate eastwards along the thermocline. The thermocline is at its shallowest in the east Pacific so changes in its depth there will have the greatest effect on the temperature at the ocean surface.

(b) Westward evolving SST event

We now consider the year 21 event; an example of an event in which SST anomalies propagate westwards across the model Pacific. At the end of year 20 the east Pacific warms. This SST anomaly then propagates westwards across the Pacific. In this section we will examine the reasons for the generation of this SST anomaly in the east Pacific and its subsequent westwards travel.

Other modelling groups (Meehl, 1990; Lau *et al*, 1992; Latif *et al*, 1993) have also reported on westward propagating SST anomalies. Neelin (1991) proposed a westward propagating SST mode which propagates westwards through changes in upwelling. This upwelling change was caused by wind stress anomalies occurring to the west of the temperature anomalies. We wish to see if similar processes take place in the UKMO model.

To understand the processes responsible for the westwards travel of the anomaly we examine differences of the various terms in the heat budget between the warm event of year 21 and the cold event of year 8. Fig. 18 shows time-longitude plots in the equatorial Pacific Ocean (10°N to 10°S) of SST anomalies for the warm event (a) and the cold event (b). As can be seen both events show westwards propagation of SST anomalies starting in the east Pacific during June or July. The SST differences between the two events for the same month in the year is shown in Fig. 18(c) and also shows westwards propagation. Examining the VAT differences (18(d)) between the two events suggests that changes in SST anomaly are not caused by changes in the thermocline depth. However there does seem to be a flattening of the thermocline across the model Pacific between the warm event and the cold event presumably due to changes in the circulation induced by the SST changes. The zonal wind stress differences (18(e)) show westwards propagation of westerly anomalies, with peak values in the wind stress occurring to the west of peak values in the SST field. This point will be returned to later.

Before further consideration of the heat budget we first consider the circumstances which lead to the existence of warm water anomalies in the east Pacific. As was discussed earlier (see figures 6 and 7) the coupled model has a significant amount of low cloud during northern summer and autumn in the region between 120°W and 90°W and 10°S and the equator. During those seasons the amount of low cloud, in that region, is significantly anti-correlated with the SST. It is possible to see that a positive feedback mechanism could exist between the SST and low cloud which would work as follows and which is shown schematically in Fig. 19;

1. Warmer SSTs cause a decrease in low level cloud or *vice versa*.

2. A decrease in low level clouds causes a decrease in shortwave top of atmosphere albedo.

3. A reduction in shortwave albedo causes increased solar heating of the ocean which in turn causes warmer SSTs.

This same process could work with cooler SSTs causing an increase in low cloud. In practice it is difficult to show cause and effect; it is better to think of this mechanism as an amplifier for anomalous SSTs or anomalous cloud amounts of either sign. However SST anomalies have a longer persistence time than do cloud anomalies and so are more likely to drive this process.

During year 20 the water in the east Pacific is anomalously warm and during SON of that year there is a large reduction in cloud in the tropical east Pacific. Fig. 20 shows total cloud, SST and total radiative heating for SON and DJF of year 20 for tropical east Pacific. As usual all plots are seasonal anomalies relative to the year 1 to 50 model seasonal climatology. In Fig. 20(a) it can be seen that there is a decrease in total cloud cover over the region of extensive low cloud in the east Pacific. Peak decreases in total fractional cloud cover are larger than 0.25 below the seasonal norm values. The largest heating anomalies averaged over the season are $40\mathrm{W/m^2}$ centred on the region of maximum cloud decrease. This large increase in ocean heating causes the SST to warm. Figures 20(c) and (d) show the SST anomaly magnitude increasing and the anomaly propagating westwards. By DJF, in the mean seasonal cycle, there is not such a large region of low cloud in the model east Pacific (see Fig. 6). Therefore the same heating anomaly will be able to generate a smaller cloud anomaly and thus a smaller radiative heating anomaly. Figures 20(b) and (f) show the reduced cloud and radiative heating anomalies for DJF.

Having established that feedbacks between SST and marine stratocumulus can act to amplify temperature anomalies in the model eastern Pacific we now continue to examine the heat budget of the model. If we assume that the entire solar heating is absorbed in a layer of depth Δz, then the heat budget equation for this layer can the be written as;

$$\int_0^{\Delta z} [\frac{\partial T}{\partial t} + \nabla \cdot (\boldsymbol{V}T)]\, dz = Q + R. \tag{1}$$

In the above equation T is the temperature, $\boldsymbol{V}$ the three dimensional ocean current, Q the heating of the ocean through the surface (referred to from now on as ocean heating) and R the residual term which includes contributions from diffusion along isopycnal surfaces, vertical diffusion, unresolved transients and failure of the assumption that all the solar heating is absorbed in the layer. The ocean heating term (Q) includes contributions from shortwave radiation fluxes (assumed to be completely absorbed in the layer), surface long wave radiation fluxes, surface latent heat fluxes and surface sensible heat fluxes.

The three possibilities that we wish to distinguish between are; (1) ocean heating; (2) advection of the mean temperature field by the anomalous velocity or (3) advection of anomalous temperature by the mean velocity field. We do this by taking 9 months of model output starting in March of year 21, the year of a warm event and computing the heat budget terms for the first 5 model layers, that is to a depth of 55.5 metres which encompasses the wind mixed layer. The same calculations are done for a cold event which also has a westward propagating anomaly from March of year 8. Having done these calculations, warm event − cold event differences in the heat budget can then be examined in order to understand the processes responsible for the movement of the SST anomalies. It is straightforward to show that the following is true;

$$\nabla \cdot (\boldsymbol{V}_w T_w) - \nabla \cdot (\boldsymbol{V}_c T_c) = 2\nabla \cdot (\boldsymbol{V}'\overline{T}) + 2\nabla \cdot (\overline{\boldsymbol{V}}T') \tag{2}$$

with

$$\overline{\boldsymbol{V}} = \frac{\boldsymbol{V}_w + \boldsymbol{V}_c}{2} \qquad \boldsymbol{V}' = \frac{\boldsymbol{V}_w - \boldsymbol{V}_c}{2}$$

and similarly for $\overline{T}$ and T'. In the above, terms which have a subscripted c refer to the cold event and terms with a subscripted w refer to the warm event. The first term on the right hand side of Eqn. 2 represents the transport of the mean temperature by the anomalous velocity field and the second term the transport of the anomalous temperature by the mean velocity field.

The terms which contribute to the warm – cold event heat budget are shown in Fig. 21 and are in order; total heating (a); advective heating (b); ocean heating (c); and the residual (d). The total heating term ($\frac{\partial T}{\partial t}$) was computed by first integrating the ocean temperature over the top five model layers using monthly mean data. These were then differenced to give the $\frac{\partial T}{\partial t}$ term. The advection terms were also computed from monthly mean data with the VT terms being integrated over the top five model levels prior to the divergence being taken. These terms and the ocean heating term were then time averaged. The residual terms were then computed using these computed terms and the heat budget equation. The contributions to the movement of the temperature anomalies were computed by first calculating each of them for each event and then taking the difference on a month by month basis for each term, e.g. to compute the advective heating difference for March, the March values for year 21 (warm event) of the advective heating are differenced from the March values of the advective heating for year 8 (cold event).

As we can see from Fig. 21 the dominant contribution to the heat budget difference in the central and western Pacific is from the advective heating term with the contribution from ocean heating only being large in the east Pacific. Over most of the east Pacific ocean heating is balanced by advective cooling. The ocean heating can be divided into heating through the surface of the ocean (21(e)) and solar heating (21(f)). The solar heating term shows a large positive anomaly from 90°W to 160°W but apart from near the coast of South America this contribution is almost canceled by increased cooling through the surface. Over most of the Pacific the residual terms are small (less than 0.2°C/100 days). There is however a period when the residual terms in the central Pacific are quite large, suggesting that the impact of diffusion or advection on timescales of less than a month could be important at that point.

Figures 21(g) and (h) show the separation of the anomalous advective term into the advection of temperature anomalies by mean velocity and the advection of the mean temperature by the anomalous velocities using Eqn. 2. To the east of the dateline the second term is the larger. To the west of the dateline the magnitude of the first term rises and becomes comparable but opposite in sign to the second term. The $\nabla \cdot (\boldsymbol{V}'\overline{T})$ tending to cool the ocean west of the dateline.

The contributions to $\nabla \cdot (\boldsymbol{V}'\overline{T})$ from the zonal, meridional and vertical components are shown in Fig. 21(i), (j) and (k) respectively. In Fig. 21(k) regions of enhanced upwelling will appear as regions of enhanced heating; more heat is being transported into the column by the increased vertical velocity. However as there is a temperature gradient with warmer water at the surface then the net effect will be to cool the column. Continuity demands that the horizontal outflow of warmer water be the same as the transport in of cooler water, thus net heat is transported out of the column.

Examination of those plots show that the changes are greatest in the zonal and vertical contributions to this term suggesting that changes in upwelling are the largest contributor to the propagating SST anomaly. These changes occur to the west of the SST anomaly and therefore cause its westward propagation. There are, however, periods and regions when the meridional component is important such as in August and September in the central Pacific. Comparison of Fig. 18(e) with that of Fig. 21(i) and (k) show that the largest changes in zonal wind stress are associated with changes in zonal current and upwelling strength. The mechanism that causes the westward transport of SST anomalies in the model is that warm anomalies induce an increase in westerly wind stress to the west of their position. These wind stress changes then cause changes in ocean currents which causes a reduction in upwelling of cool water from below and thus an increase in the surface temperature. Gill (1980) showed that warm tropical anomalies will cause anomalous westerly flow near the surface to the west of that anomaly. This flow will cause an increase in westerly wind stress on the ocean.

To summarize; the warm event is initiated by warmer SST causing a reduction in low cloud cover. The increased radiative heating warms the shallow mixed layer and causes a further increase in SST. The positive feedback loop continues with an approximately seasonal timescale. SST anomalies then propagate westwards; their transport mainly being driven by changes in the advective heating term in the heat budget equation. These changes in the central and eastern Pacific are largely due to the effect of anomalous velocities acting on the mean temperature field.

Changes in upwelling and zonal velocity are the largest contributors to the anomalous velocity part of the heat budget term and these changes are caused by increases in westerly zonal wind stress occurring to the west of the warm temperature anomalies.

(c) All events

We have examined two events and established that there are two possible mechanisms acting: one in which warm SST anomalies cause an increase in westerly windstress to the west of them and another in which an eastwards propagating Kelvin wave triggers warming over the central and eastern Pacific. We now examine all the model events and show that their behaviour can be understood in terms of these two mechanisms. We also confirm that the marine stratocumulus feedback discussed earlier occurs in other events than the year 21 warm event. To do this we examine monthly anomalies in the equatorial region (10°N to 10°S) of the following quantities: VAT (vertically averaged temperature) to a depth of 360 m in the east(120°W to 90°W), central(180° to 150°W) and west Pacific(120°E to 150°E) and SST in the same regions. We also examine seasonal anomalies of low level cloud for the region of extensive cloud in the east Pacific (0° to 10°S and 120°W to 100°W). If the Kelvin wave mechanism is operating then there will be transfer of VAT from west Pacific to east Pacific. In warm events where SST anomalies propagate westwards then the coupled SST wind stress mechanism is active. Fig. 22 shows these plots for all model warm events.

By examining the plots and in particular the positions of the maximum values associated with a warm event the events can be classified. The year 1 warm event (22(a)) is clearly a Kelvin wave event with VAT anomalies propagating eastwards and the central and eastern Pacific warming at approximately the same time. The year 38 event (22(f)) also shows a propagating Kelvin wave signal with SST anomalies moving eastwards. The year 43 event (22(g)) is another Kelvin wave event with warming of the central and eastern Pacific occurring at approximately the same time. The year 47 event (22(h)) is similar to the year 43 event. Considering now the year 10 event – this event is an example of an event where both mechanisms are active. The Kelvin wave reaches the east Pacific in JJA of year 9; there it causes an increase in SST. The warm SST in DJF of year 9/10 causes the cloud feedback mechanism discussed earlier to become active and causes heating of the ocean. The warm water then propagates westwards. A similar thing happens in year 4 with warm water propagating westwards with cloud amplification of east Pacific SST anomalies being a factor in generating the warmer SSTs. The start position of the eastwards propagating VAT anomaly varies between events. In all these events the VAT anomaly seems to be triggered by anomalously westerly wind stress. The position and magnitude of these wind stress anomalies varies between 120°E and the dateline and in many cases are small in latitudinal extent.

The year 21 and 17 events are both westward propagating events. The year 21 event has been discussed earlier. The year 17 event is part of a long period of anomalously warm conditions in the eastern Pacific. During this period the low level cloud is reduced and the east Pacific VAT is greater than normal. In all but the year 38 and year 47 warm events, low cloud is reduced and presumably affects the SST through the feedback mechanism discussed earlier.

In all events except the year 21 event the peak warming, in the eastern Pacific, occurs in the second half of the year (June to December). In five of the events the peak warming occurs in June to September and there appears to be a strong coupling to the seasonal cycle.

In summary the predominant mechanism for a warm event is that of eastwards propagating Kelvin waves triggering warming over the eastern and central Pacific. A westwards propagating SST was also observed in the model. The anomalous SST propagates mainly by changes in upwelling and zonal currents driven by changes in the zonal wind stress. Reductions in low level marine stratocumulus also seem to occur in many events and could be a possible amplifying factor for the strength of the SST anomaly.

5 Response to CO_2 increase

In this section the effects of increasing concentrations of atmospheric CO_2 on the model ENSO-like variability is considered. Prior to this section we have only considered the control experiment; recall that in the transient experiment atmospheric CO_2 was increased at a rate of 1%(compounded) per year.

The definition of a warm and cold event that we have used before has been in terms of anomalies relative to a 50 year mean. For a transient run where the temperature increases with time this definition is inadequate; warm anomalies will occur later in the integration and cool anomalies earlier in the integration. We must adopt a definition closer to the physics of what we are attempting to understand. Recall Fig. 8(b) where power spectra of the mean temperature in the Nino3 region and of the SOI were shown for the model. Most of the power is in frequencies of less than 80 months. We therefore work in terms of anomalies defined relative to a centred 11 year moving average. That is an anomaly at time T is defined relative to the mean for the period $T-5$ years and $T+5$ years. Compare this to Meehl *et al* (1993) where two coupled model experiments are described; one in which atmospheric CO_2 was instantaneously doubled and another in which atmospheric CO_2 was held constant. Anomalies for each experiment in that paper were defined relative to the mean climatology of each experiment.

A further problem in the model integration described in this paper was that in the last 10 years of the transient experiment, centred on the time of doubling, there is only one strong event (as defined earlier) and therefore any changes in the model ENSO response are unlikely to be statistically significant. Therefore, we consider changes in the variance on the one to 10 year timescale. This is just the power in the one to 10 year timescale. We wish to consider how this changes with time in both the transient and control runs.

Therefore for each time, T, we take data from the 11 year period $T-5$ to $T+5$ and detrend these data on a point by point basis. From these detrended data we compute the standard deviation. This is done for all points and for all times from year 5 to year 70, using DJF data from year 0 to year 75 of the both the control and transient integration. DJF data is used because the peak affect of a warm ENSO event occurs at this time. Fig. 23(a) and (c) shows time-longitude plots of the differences between the transient and the control experiments of the 11 year means for SST and total precipitation averaged over the region between 10°N and 10°S. Fig. 23(b) and (d) show similar time-longitude plots for the standard deviation computed over 11 year periods for the transient run divided by the variability in the equivalent period for the control run.

Examining first the SST changes (23(a) and (b)) we find that the warming due to increased atmospheric CO_2 occurs most quickly in Indonesia, the east Pacific and the east Atlantic and least quickly in the central Pacific, west Indian and west Atlantic regions. The temperature difference between the west and east Pacific shows very little change. There are no significant changes in the variability (though to detect that changes of 20% variance are significant at the 5% level requires at least 83 degrees of freedom). There does not even seem to be a trend in the variance changes. We therefore conclude that there is no reason to believe that the magnitude of the SST anomalies will change as atmospheric concentrations of CO_2 change. It should be stressed that this result is extremely tentative, more statistics are required to have greater confidence in this result. Meehl *et al* (1993) in their coupled model, in which the SST changes associated with the ENSO cycle are confined to the west Pacific, find that there is no change in frequency or strength of their model events. The results presented here are consistent with their findings.

Considering next the precipitation changes (Fig. 23(c) and (d)) we see that precipitation increases in the Indonesian/Indian Ocean region as CO_2 increases and precipitation decreases in the west central Pacific Ocean and over South America. Changes in variability, like the SST changes, are not significant (at the 5% level). However there is some hint of increased variability over the region where total precipitation has increased and perhaps over the east Atlantic Ocean. The model has an increase in interannual precipitation variability where total precipitation increases. Meehl and Washington (1993) reported on the results of a coupled model

where atmospheric CO_2 was double present values and showed that there was an increase in both the amount of Indian summer monsoon precipitation and in the variability of that precipitation compared to the experiment where CO_2 was at present values. Meehl *et al* (1993) also found that the magnitude of the changes in modelled precipitation during ENSO events would be greater in a climate with doubled atmospheric CO_2.

6 Conclusion

The UKMO model has an oscillation that is qualitatively similar to that of the observed ENSO. The model is a global coupled atmosphere ocean GCM and uses flux correction to keep the control climate close to that observed. The model oscillation is weaker by approximately a factor of 2 compared to that observed whereas the model ENSO timescale is longer than that observed. Changes in pressure patterns, precipitation and SST during warm and cold events are similar in both the model and the observed data.

Two types of model ENSO events occur; one in which SST anomalies propagate westwards and another in which the central and eastern Pacific warms at approximately the same time. Six of the eight model model events are of predominantly the second type.

The westward propagation of SST anomalies is caused by these anomalies inducing westerly windstress anomalies to the west of their position. This anomalous windstress causes changes in near surface ocean currents which reduces upwelling strength and thus causes the surface layer to the west of the warm SST anomaly to warm.

The second type of event is triggered by eastwards propagating Kelvin waves which cause the thermocline to deepen in the east Pacific, thus causing the surface layer to warm. There is no evidence of these waves generating westward traveling Rossby waves on the eastern coast of the model Pacific. In this type of event the peak temperature anomaly in the eastern Pacific Ocean has some phase locking to the seasonal cycle.

In the model, marine stratocumulus clouds play an amplifying role as increases in SST can cause reductions in cloud and thus enhanced solar heating. The model, however has its marine stratocumulus displaced too far to the west and equatorwards compared to the position of the observed clouds. There is some evidence from the literature of a link between marine stratocumulus and SST anomalies. Hanson (1991) using COADS cloud data and SST anomalies found that marine stratocumulus amounts were anomalously low above positive SST anomalies. Weare (1992) by using cloud amounts estimated from Nimbus-7 also showed a negative correlation between cloud and SST anomalies in the east Pacific marine stratocumulus regions. Peterson *et al* (1992) examined the relationship between SST and low cloud, amongst others, for both observed data and the Hamburg GCM. For the observations they found that increases in SST in the marine stratocumulus regions caused a decrease in cloud. Klein and Hartmann (1993) related changes in static stability to changes in stratocumulus cloud. Furthermore they found that the four years (1957, 1965, 1972 and 1976) in the period 1950 – 1981 with the smallest amounts of cloud in the region between 0° and 10°S and 80°W and 100°W were El Niño years.

The effect of increasing atmospheric CO_2 on the standard deviation computed over the one to 10 year period was examined. For both precipitation and SST there were no statistically significant changes in this quantity. Furthermore the SST standard deviation showed no trend unlike the precipitation variance which showed some evidence of a tendency to increased variability over the Indonesian/Indian Ocean regions. Based on this there is no reason to believe that the strength of peak SST anomalies in the ENSO cycle will change as atmospheric CO_2 increases.

Acknowledgments

I would like to thank Drs J.F.B. Mitchell, M. Davey, P. Rowntree, C. Gordon, A. Slingo and many other colleagues for helpful discussions. The ERBE data were obtained from World Data Centre A, at the NASA Goddard Space Flight Center. Ms K. Maskell and Mr M. N. Ward provided me,

in an appropriate format, with much of the observed data used in this paper. Jonathan Gregory, Mark Webb and I developed much of the software used to produce the figures in this paper; I would like to thank them for this work. James Murphy carried out the model integrations used in this study. This work was supported by the U.K. Department of the Environment under contract number PECD 7/12/37.

Bibliography

Barnett, T. P., M. Latiff, E. Kirk, and E. Roeckner, 1991: On ENSO physics. *J. Climate*, **4**, 487–515.

——, A. D. D. Genio, and R. A. Reudy, 1992: Unforced decadal fluctuations in a coupled model of the atmosphere and ocean mixed layer. *J. Geophys. Res.*, **97**(C5), 7341–7354.

Bjerknes, J., 1966: Survey of El-Niño 1957–1958 in its relationship to tropical Pacific meteorology. *Inter-American Tropical Tuna commission, Bull*, **12**(2), 25–86.

——, 1969: Atmospheric teleconections from the equatorial Pacific. *Monthly Weather Review*, **97**(3), 163–172.

Bottomley, M., C. K. Folland, J. Hsiung, R. E. Newell, and D. E. Parker, 1990: *Global Ocean Surface Temperature Atlas*. HMSO, London. Publication funded by UK depts of Energy and Environment.

Bryan, K., and M. D. Cox, 1972: An approximate equation of state for numerical models of ocean circulation. *J. Phys. Oceanogr.*, **2**, 510–514.

Cane, M. A., and D. W. Moore, 1981: A note on low-frequency equatorial basin modes. *J. Phys. Oceanogr.*, **11**, 1578–1584.

Cox, M. D., 1984: A primitive equation, three dimensional model of the ocean. GFDL Ocean Group Technical Report 1, GFDL.

Gill, A. E., 1980: Some simple solutions for heat-induced tropical circulation. *Quart. J. R. Met. Soc*, **106**, 447–462.

Glantz, M. H., R. W. Katz, and N. Nicholls, editors, 1991: *Teleconnections linking Worldwide Climate anomalies*. Cambridge University Press.

Gordon, C., 1989: Tropical ocean-atmosphere interactions interactions in a coupled model. *Phil. Trans. R. Soc. Lond. A*, **329**, 207–223.

Gregory, D., and P. R. Rowntree, 1990: A mass flux convection scheme with representation of cloud ensemble characteristics and stability-dependent closure. *Monthly Weather Review*, **118**(7), 1483–1506.

Halpern, D., R. A. Knox, D. S. Luther, and S. G. H. Philander, 1989: Estimates of equatorial upwelling between 140° and 110°W during 1984. *J. Geophys. Res.*, **94**(C6), 8018–8020.

Hanson, H. P., 1991: Marine stratocumulus climatologies. *Int. J. Climatol.*, **11**, 147–164.

Harrisson, E. F., P. Minnis, B. R. Barkstrom, V. Ramanathan, R. D. Cess, and G. G. Gibson, 1990: Seasonal variation of cloud radiative forcing derived from the earth radiation budget experiment. *J. Geophys. Res.*, **95**(D11), 18687–18703.

Hellerman, S., and M. Rosenstein, 1983: Normal monthly wind stress over the world ocean with error estimates. *Journal of Physical Oceanography*, **13**, 1093–1104.

Hulme, M., 1992: A 1951-80 global land precipitation climatology for the evaluation of general circulation models. *Climate Dynamics*, **7**, 57–72.

Klein, S. A., and D. L. Hartmann, 1993: The seasonal cycle of low stratiform clouds. *J. Climate*, **6**(8), 1587–1606.

Kousky, V. E., and A. Leetmaa, 1989: The 1986–1987 Pacific warm episode: Evolution of oceanic and atmospheric anomaly fields. *J. Climate*, **2**, 254–267.

Kraus, E. B., and J. S. Turner, 1967: A one dimensional model of the seasonal thermocline. Part II. *Telus*, **19**, 98–105.

Latif, M., A. Sterl, E. Maier-Reimer, and M. M. Junge, 1993: Climate variability in a coupled GCM. Part I: The tropical Pacific. *J. Climate*, **6**, 5–21.

Lau, N.-C., S. G. H. Philander, and M. J. Nath, 1992: Smulation of ENSO-like phenomena with a low-resolution coupled GCM of the global ocean and atmosphere. *J. Climate*, **5**, 284–307.

Lau, K.-M., 1981: Oscillations in a simple equatorial climate system. *J. Atmos. Sci.*, **38**, 248–261.

Levitus, S., 1982: Climatological atlas of the world ocean. Professional Paper 13, National Oceanic and Atmospheric Administration, Rockville, Maryland.

Manabe, S., R. J. Stouffer, M. J. Spelman, and K. Bryan, 1991: Transient responses of a coupled ocean-atmosphere model to gradual changes of atmospheric CO_2. Part I: annual mean response. *J. Climate*, **4**(8), 785–818.

Meehl, G. A., and W. M. Washington, 1993: South asian summer monsoon variability in a model with doubled atmospheric carbon dioxide concentration. *Science*, **206**, 1101–1104.

——, G. W. Branstator, and W. M. Washington, 1993: Tropical Pacific interannual variability and CO_2 climate change. *J. Climate*, **6**, 42–63.

——, 1990: Seasonal cycle forcing of El-Niño-Southern Oscillation in a global, coupled ocean-atmosphere GCM. *J. Climate*, **3**, 72–98.

Murphy, J. M., and J. F. B. Mitchell, 1994. Transient response of the Hadley Centre coupled ocean-atmosphere model to increasing carbon dioxide. Part II: Spatial and temporal structure of response. (Submitted to *J. Climate*).

——, 1994. Transient response of the Hadley Centre coupled ocean-atmosphere model to increasing carbon dioxide. Part I: control climate and flux correction. (Submitted to *J. Climate*).

Nagai, T., T. Tokioka, M. Endih, and Y. Kitamura, 1992: El Niño-Southern Oscillation simulated in an MRI atmosphere-ocean coupled general circulation model. *J. Climate*, **5**, 1202–1233.

Neelin, J. D., M. Latif, M. A. F. Allart, M. A. Cane, U. Cubasch, W. L. Gates, P. R. Gent, C. Gordon, C. R. Mechoso, G. A. Meehl, J. M. Oberhuber, S. G. H. Philkander, P. S. Schopf, K. R. Sperber, A. Sterl, T. Tokioka, J. Tribbia, and S. E. Zebiak, 1992: Tropical air-sea interaction in general circulation models. *Climate Dynamics*, **7**, 73–104.

——, 1991: The slow sea surface temperature mode and the fast-wave limit: Analytic theory for tropical interannual oscillations and experiments in a hybrid coupled model. *J. Atmos. Sci.*, **48**(4), 584–606.

Pacanowski, R. C., and S. G. Philander, 1981: Parameterization of vertical mixing in numerical models of tropical oceans. *J. Phys. Oceanogr.*, **11**, 1443–1451.

Palmer, T. N., G. J. Shutts, and R. Swinbank, 1986: Alleviation of a systematic westerly bias in general circulation and numerical weather prediction models through an orographic gravity wave drag parameterization. *Quart. J. R. Met. Soc.*, **112**, 1001–1039.

Parker, D., C. K. Folland, M. N. Ward, A. Bevan, M. Jackson, and K. Maskell, 1993: Marine surface data for analysis of climate fluctuations on interannual to century timescales. In *Proc. National Academy of Science National Research council workshop on climate variability on Decade to Centuary time scales, Irvine, Cal., USA, 21-25 Sept 1992.*

Peterson, T. C., T. P. Barnett, E. Roeckner, and T. H. Vonder Haar, 1992: An analysis of the relationship between cloud anomalies and sea surface temperature anomalies in a global circulation model. *J. Geophys. Res.*, **97**(D18), 20497–20506.

Philander, S. G. H., and A. D. Seigel, 1985: Simulation of El Niño of 1982–1983. In Nihoul, J., editor, *Coupled Ocean/Atmosphere models*, volume 40 of *Oceanography Series*, 517–541. Elsivier.

——, R. C. Pacanowski, N.-C. Lau, and M. J. Nath, 1992: Simulation of ENSO with a global atmosphere GCM coupled to a high-resolution tropical Pacific ocean GCM. *J. Climate*, **5**, 308–329.

Rasmusson, E. M., and T. H. Carpenter, 1982: Variations in tropical sea surface temperature and surface wind fields associated with the Southern Oscillation/El-Niño. *Monthly Weather Review*, **110**, 354–384.

Rebert, J. P., J. R. Donguy, G. Eldin, and K. Wyrtki, 1985: Relations between sea level, thermocline depth, heat content, and dynamic height in the tropical Pacific ocean. *J. Geophys. Res.*, **90**(C6), 11719–11725.

Redi, M. H., 1982: Oceanic isopycnal mixing by coordinate rotation. *J. Phys. Oceanogr.*, **12**, 1154–1158.

Roberts, D. L., and H. Cattle, 1989: Simulation of sea-ice in a coupled atmosphere-ocean model. Met O 20 DCTN 85, Meteorological Office, London Rd, Bracknell, Berkshire, RG12 2SY.

Ropelewski, C. F., and M. S. Halpert, 1987: Global and regional scale precipitation patterns associated with the EL Niño/Southern Oscillation. *Monthly Weather Review*, **115**, 1606–1626.

——, and ——, 1989: Precipitation patterns associated with the high index phase of the southern oscillation. *J. Climate*, **2**, 268–284.

Rowntree, P. R., 1972: The influence of tropical east Pacific Ocean temperatures on the atmosphere. *Quart. J. R. Met. Soc.*, **98**, 290–321.

Semtner, A. J., 1976: A model for the thermodynamic growth of sea ice in numerical investigation of climate. *J. Phys. Oceanogr.*, **6**, 379–389.

Senior, C. A., and J. F. B. Mitchell, 1993: Carbon dioxide and climate: The impact of cloud parameterization. *J. Climate*, **6**, 393–418.

Slingo, A., and D. W. Pearson, 1987: A comparison of the impact of an envelope orography and of a parameterization of orographic gravity-wave drag on model simulations. *Quart. J. R. Met. Soc.*, **113**, 847–870.

——, R. Wilderspin, and R. N. B. Smith, 1988: The effect of improved parameterizations on simulations of cloudiness and the earth's radiation budget in the tropics. *J. Geophys. Res.*, **94**, 2281–2301.

Smith, R. N. B., 1990: A scheme for predicting layer clouds and their water content in a general circulation model. *Quart. J. R. Met. Soc.*, **116**, 435–460.

Sperber, K. R., and S. Hameed, 1991: Southern oscillation simulation in the OSU coupled upper ocean-atmosphere GCM. *Climate Dynamics*, **6**, 83–97.

Stockdale, T. et al., 1993: Intercomparison of tropical ocean GCMs. WCRP 79, World Climate Programme.

Suarez, M. J., and P. S. Schopf, 1988: A delayed action oscillator for ENSO. *Journal of Atmospheric Sciences*, **45**, 3283–3287.

Walker, G. T., and E. W. Bliss, 1930: World weather IV. *Mem. Roy. Meteor. Soc.*, **3**, 81–95.

Ward, M. N., 1992: Provisionally corrected surface wind data, worldwide ocean-atmosphere surface fields, and sahelian rainfall variability. *J. Climate*, **5**, 454–475.

Warrilow, D., A. B. Sangster, and A. Slingo, 1986: Modelling of land surface processes and their influence on European climate. Met O 20 DCTN 38, Meteorological Office, London Rd, Bracknell, Berkshire, RG12 2SY.

Weare, B. C., 1992: Variations in *Nimbus*-7 cloud estimates. Part II: regional changes. *J. Climate*, **5**, 1506–1513.

Wilson, M. F., and A. Henderson-Sellers, 1985: A global archive of land cover and soils data for use in general circulation climate models. *Journal of Climatology*, **5**, 119–143.

Wyrtki, L., and B. Kilonsky, 1984: Mean water and current structure during the Hawaii-to-Tahiti shuttle experiment. *J. Phys. Oceanogr*, **14**, 242–253.

Wyrtki, K., 1984: The slope of sea level along the equator during the 1982/1983 El Niño. *J. Geophys. Res.*, **89**(C6), 10419–10424.

Zebiak, S. E., and M. A. Cane, 1987: A model El Niño–Southern Oscillation. *Monthly Weather Review*, **115**(10), 2262–2278.

——, 1986: Atmospheric convergence feedback in a simple model for El Niño. *Monthly Weather Review*, **114**, 1263–1271.

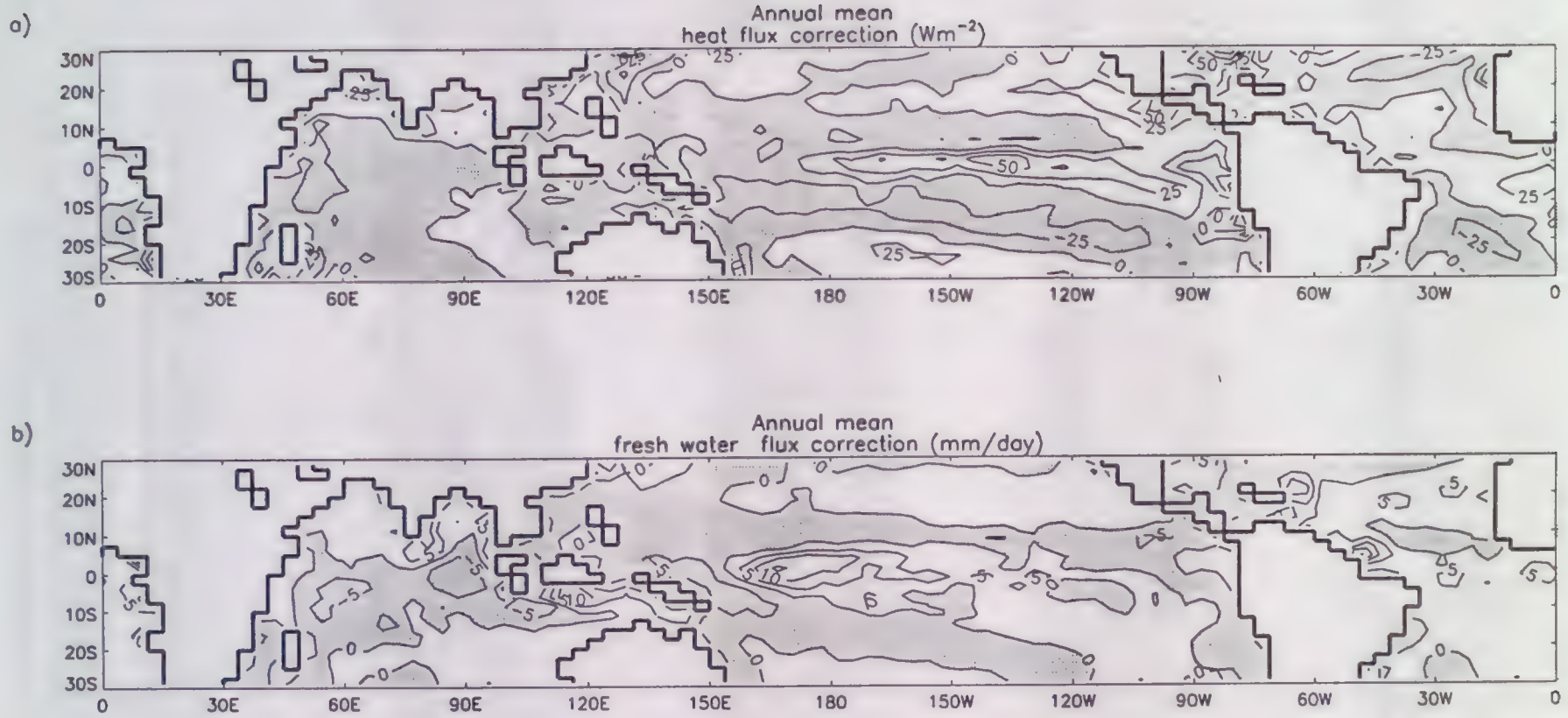

Figure 1: Heat and fresh water flux corrections

Plot (a): annual mean of heat flux correction. Plot (b): annual mean fresh water flux correction. In (a) a contour interval of 25Wm^{-2} is used while in (b) a contour interval is 5.0 mm/day is used. In both plots stippling is used for negative flux corrections.

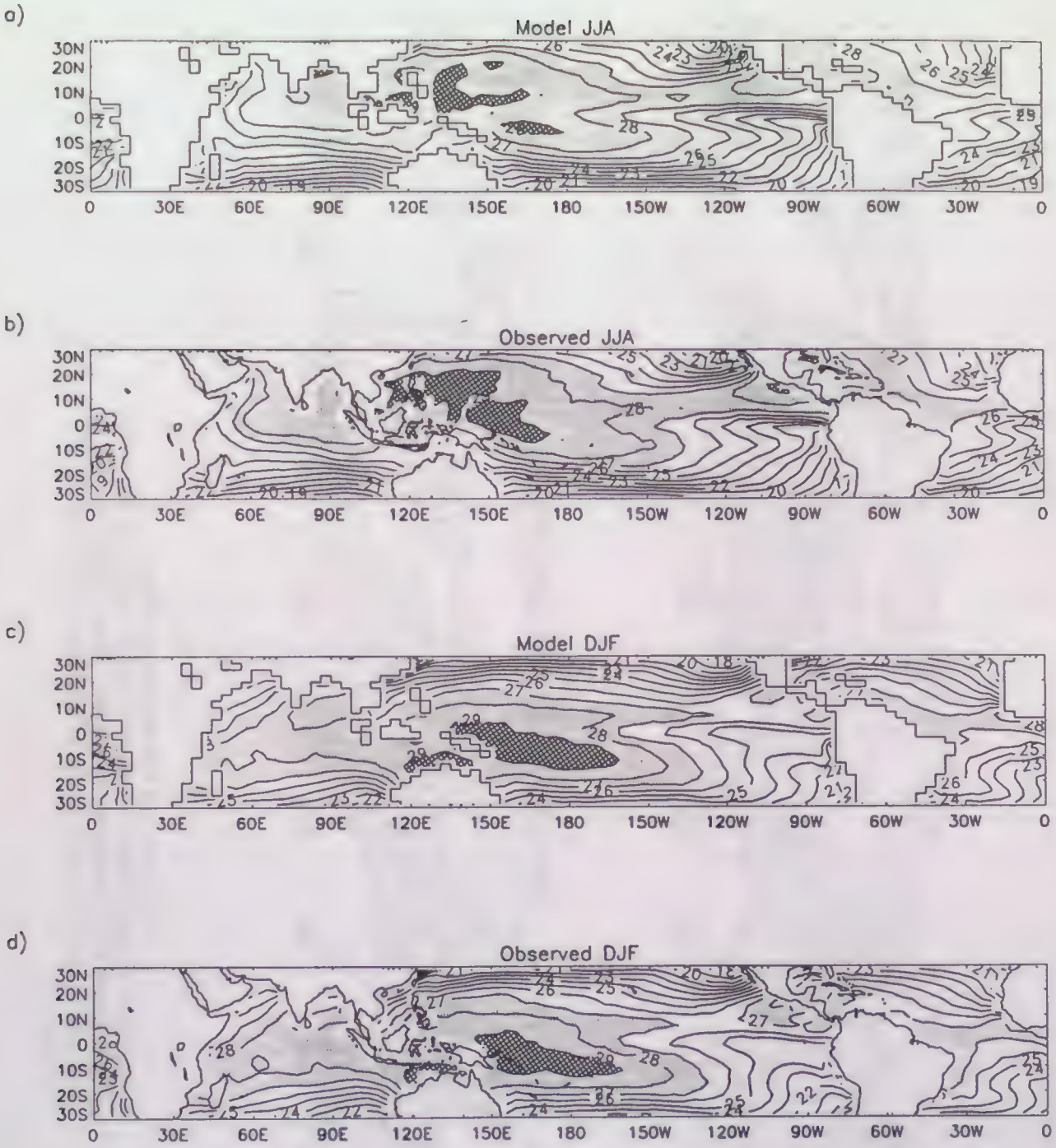

Figure 2: Model and observed climatologies of sea surface temperature
Figure (a) shows the mean JJA tropical sea surface temperature from the first 50 years of the integration (b) shows the equivalent observed field from the period 1948–1988.
(c) shows the model DJF tropical sea surface field from the same period as (a) while (d) shows the observed field for DJF using the same period as (b).
The contour interval for all plots is 1°C with stippling for temperatures greater than 27°C and cross hatching for temperatures greater than 29°C.

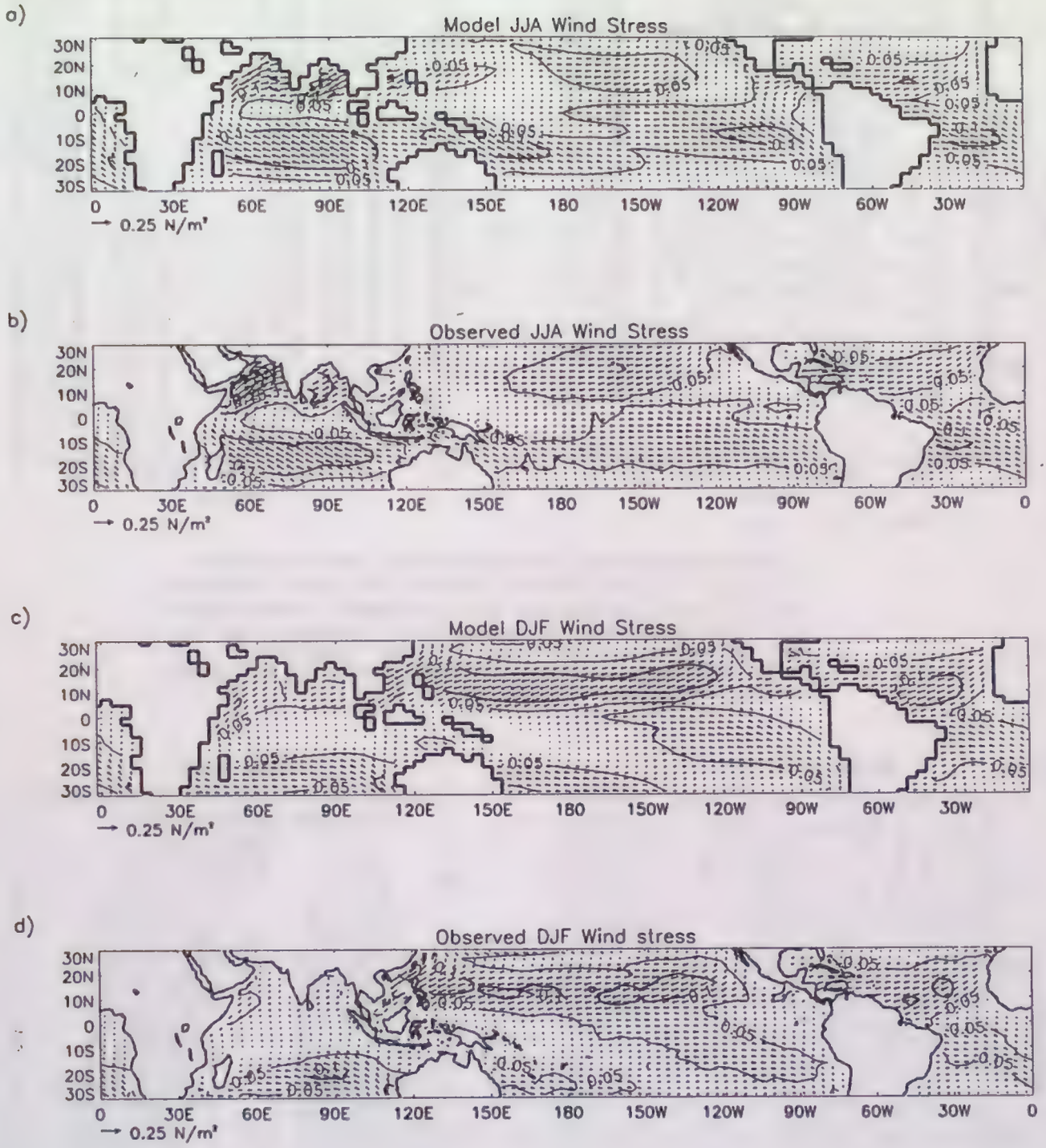

Figure 3: Observed and Model wind stresses for JJA and DJF

Figures (a) and (c) show the model climatology of surface wind stress over the tropical regions for JJA and DJF respectively. Figures (b) and (d) show the observed windstress from Hellerman and Rosenstein (1983) for JJA and DJF respectively scaled by a factor of 0.75.

In all plots scaling arrows are displayed in the left hand corner. The contours are of magnitude with an interval of $0.05 \mathrm{Nm}^{-2}$.

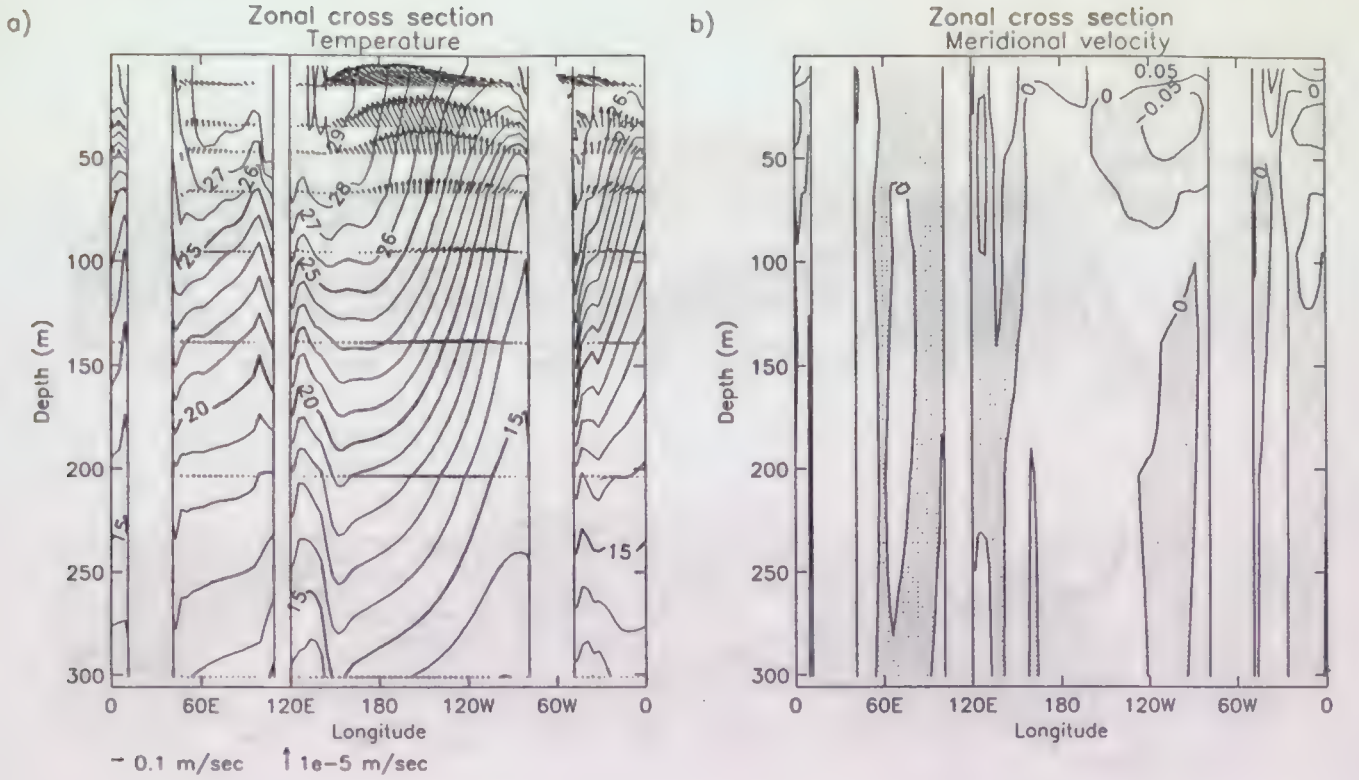

Figure 4: Equatorial annual mean temperature and velocity cross sections
All cross sections are averages between 1.25°N to 1.25°S. Plot (a): temperature, zonal velocity and vertical velocity over the equatorial region. The contour interval is 1°C with every fifth contour line in bold. Velocity components are shown by vector arrows with the vertical component considerably exaggerated.
Plot (b): meridional velocity with a contour interval of 0.05 m/s and stippling used for southwards flow.

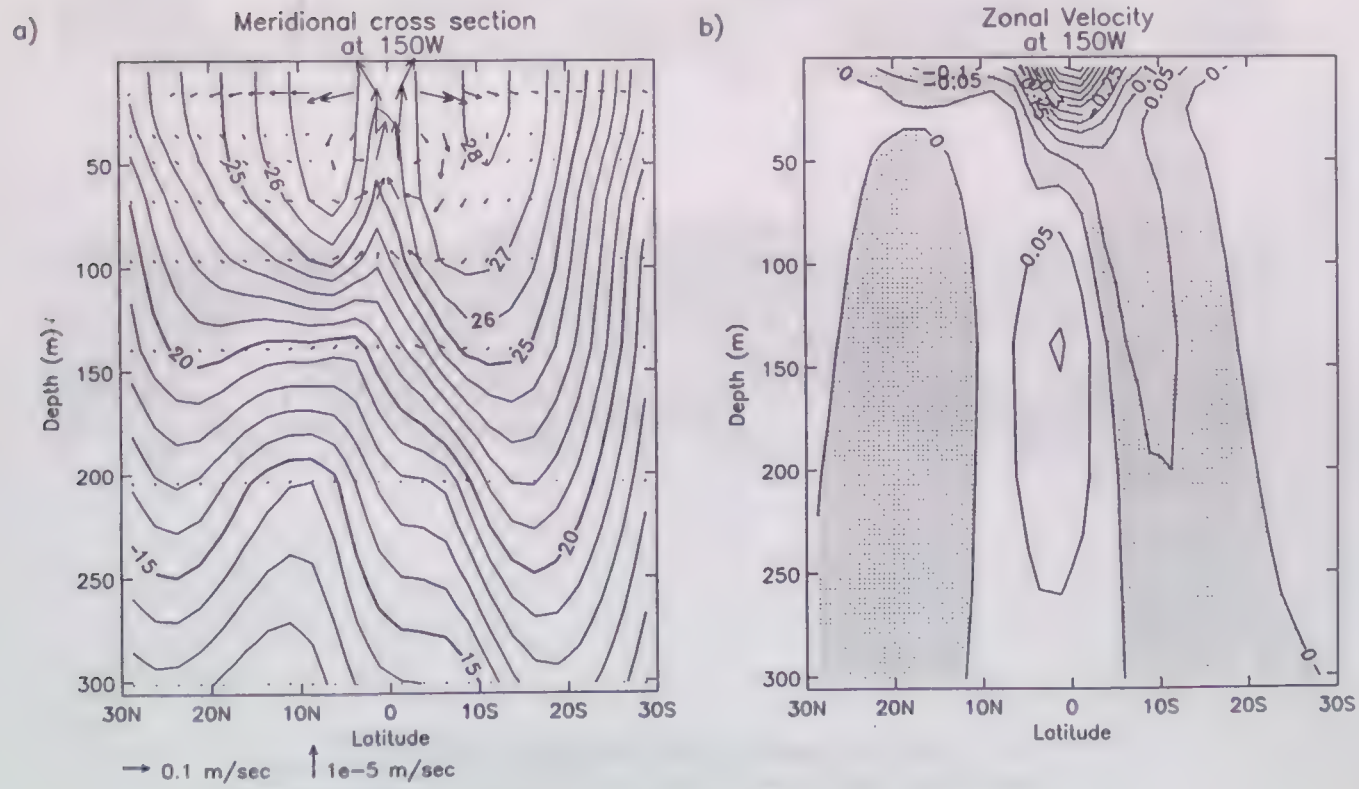

Figure 5: Annual mean meridional cross sections
Plot (a) shows a contour plot of annual mean temperature at 150°W, with a contour interval of 1°C. Every fifth contour is drawn in bold. Also shown in this plot are the vertical and meridional components of velocity as vector arrows with the vertical component considerably exaggerated.
Plot (b) shows a contour plot of zonal velocity at 150°W with a contour interval of 0.05 m/s. Easterly values are shown stippled.

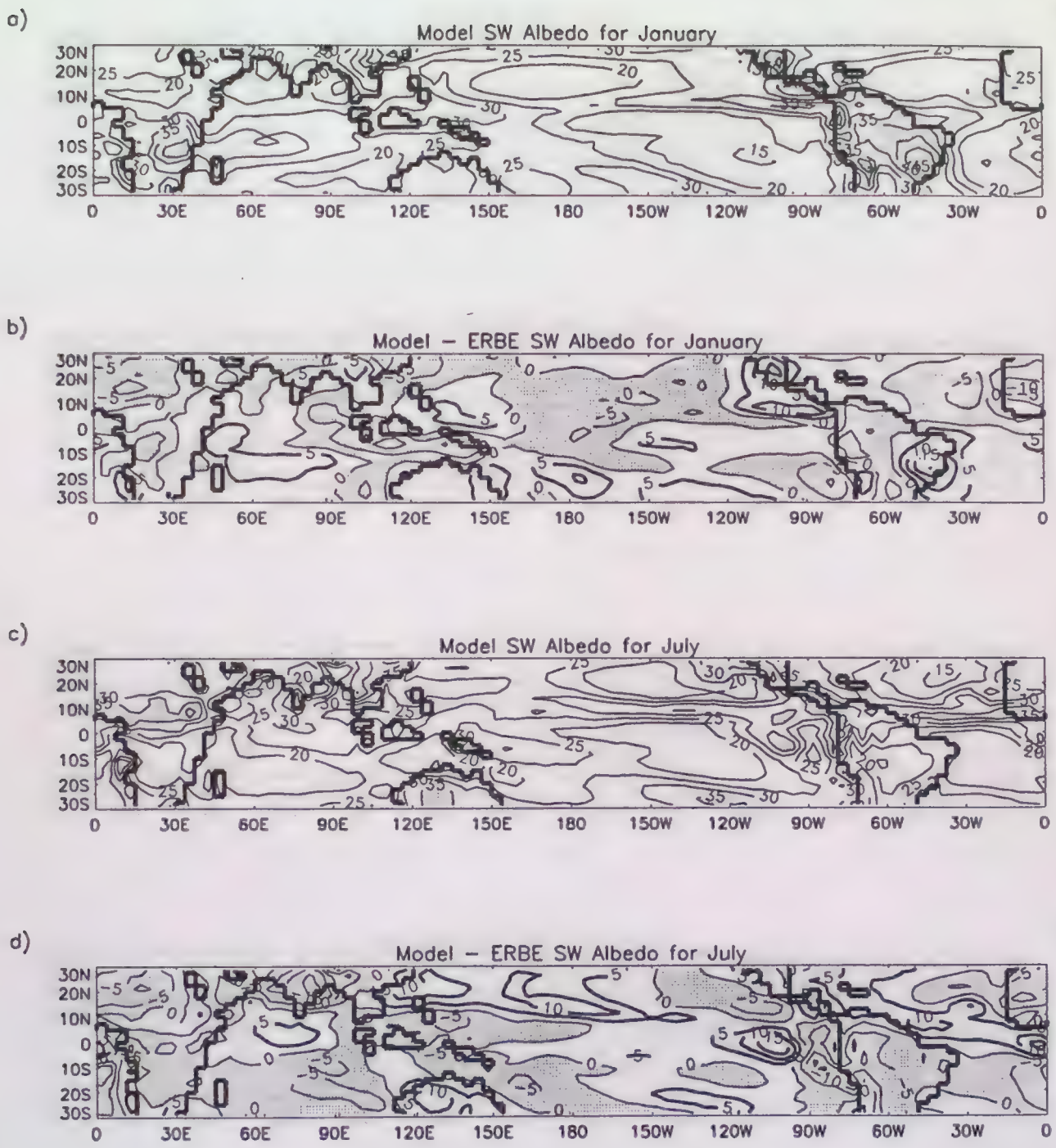

Figure 6: Model short wave albedos

Plots (a) and (c) show the model climatology of the short wave albedo in the tropics for January and July. A contour interval of 5% is used with stippling showing regions where the albedo is greater than 35%.

Plots (b) and (d) show the differences between the model climatology and the ERBE climatology for the same months. A contour interval of 5% is used with stippling for negative differences.

All plots have been smoothed using a 1-2-1 smoother in each direction prior to plotting. The model data are from the first 50 years of the control integration while the ERBE data are from the period July 1985 to January 1989.

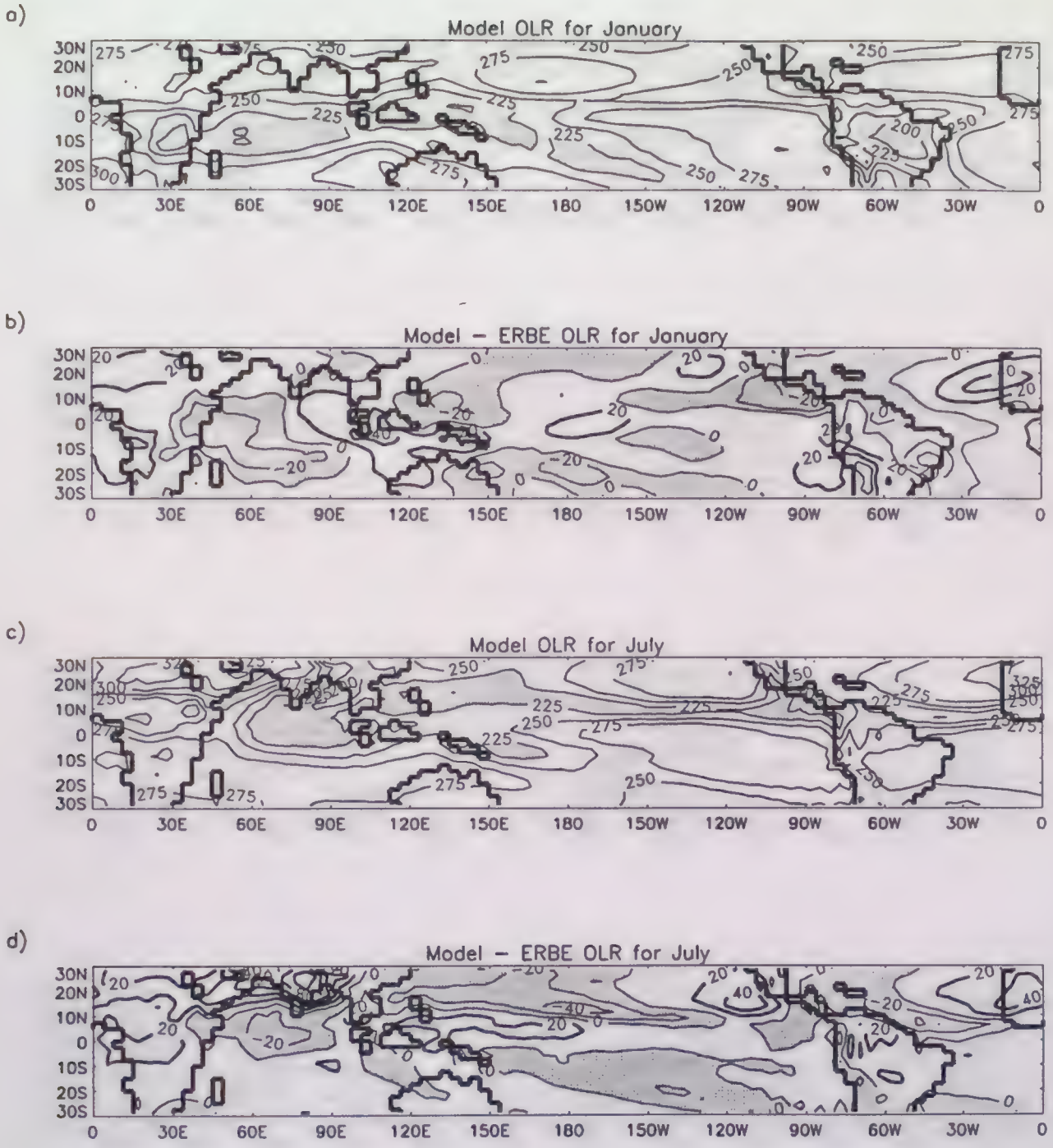

Figure 7: Outgoing Longwave Radiation

The plots are the same as 6 except that outgoing longwave radiation is displayed. Contours are every $25 W/m^2$ with stippling below $225 W/m^2$. In the difference plots a contour interval of $20 W/m^2$ is used with stippling for negative differences. All plots have been smoothed using a 1-2-1 smoother in each direction prior to plotting.

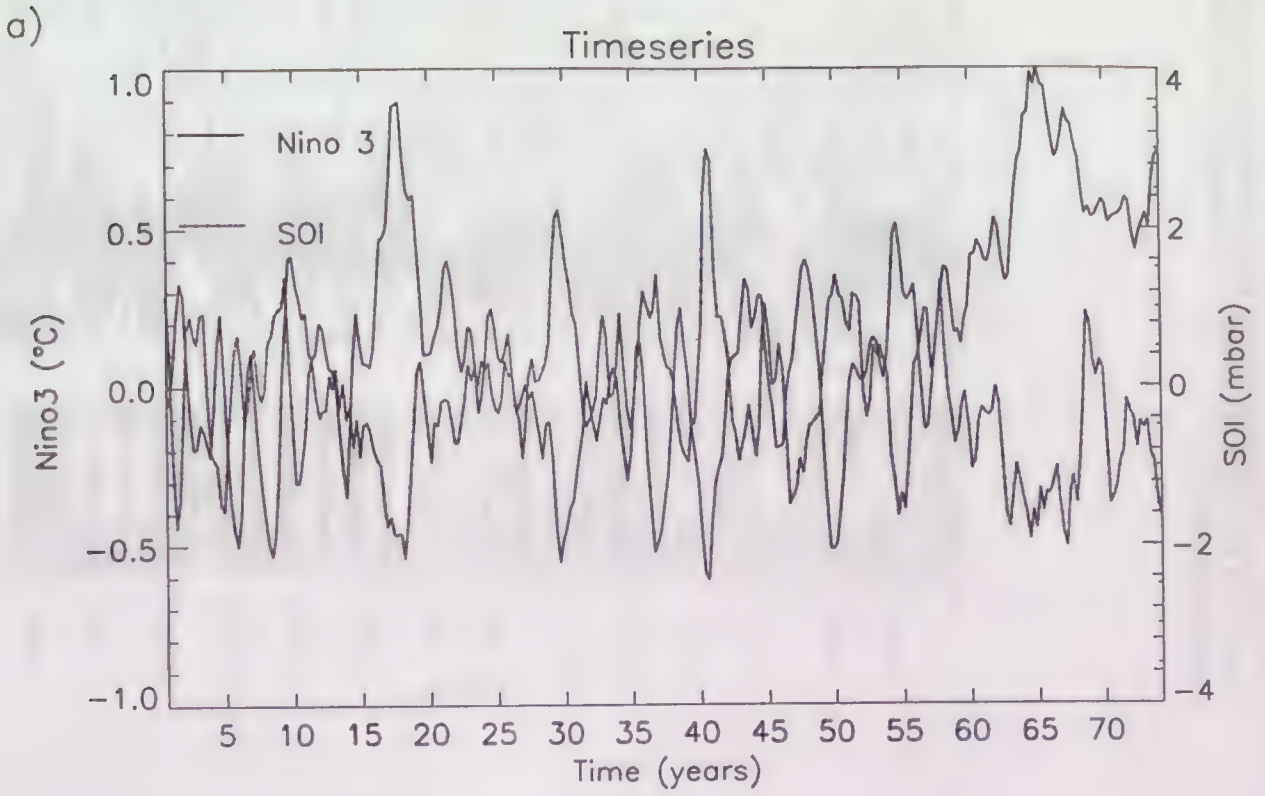

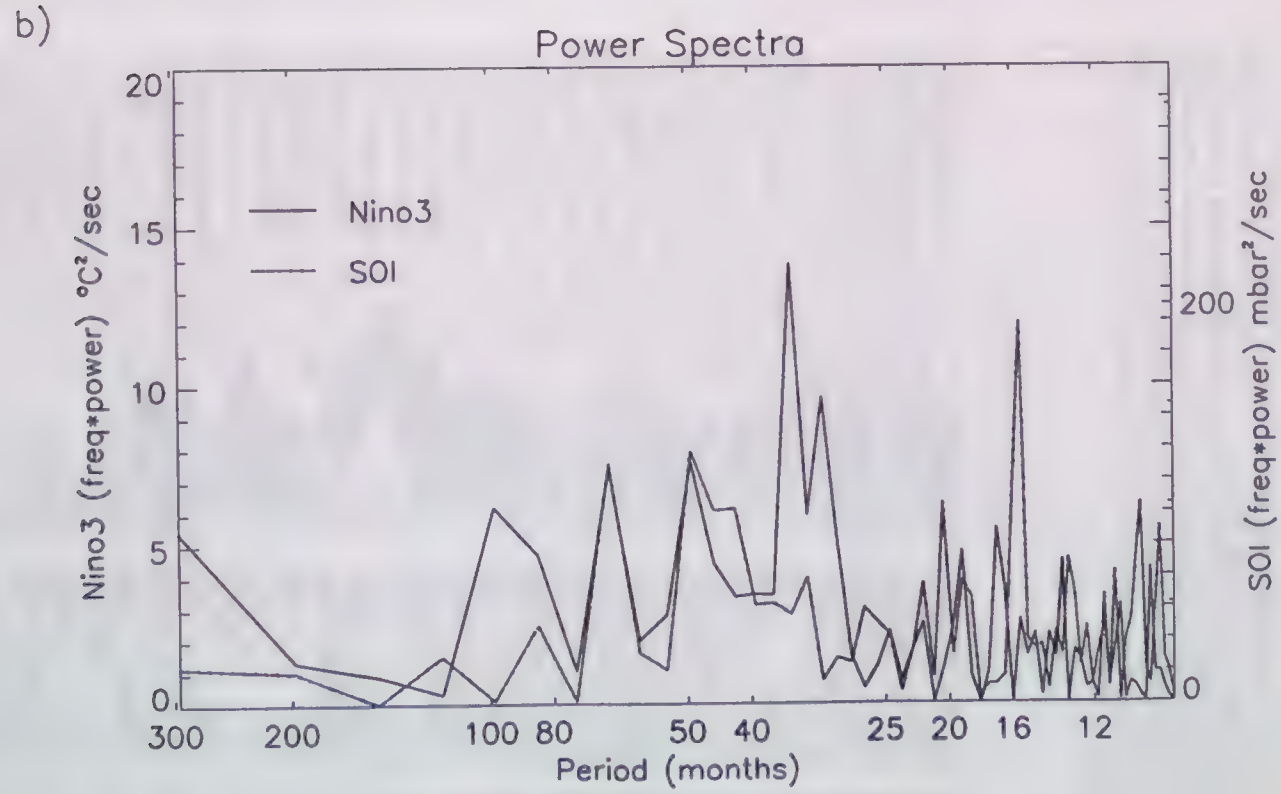

Figure 8: SOI and Nino3 timeseries and power spectra

Figure (a) is a timeseries of the seasonal temperature anomaly for the model Nino3 region (solid line) and southern oscillation index (SOI) (dashed line) for the 75 years of the control run. The righthand axis refers to the SOI timeseries, while the lefthand axis refers to the Nino3 temperature timeseries.

Figure (b) shows the power spectra of the Nino3 (solid line) temperature and the SOI (dashed line) from years 1 to 50 of the model integration. The ordinate is the frequency (ω) multiplied by the estimate of the power at that frequency.

Figure 9: Modelled time/longitude plot of sea surface temperatures
This plot shows a time/longitude plot for the equatorial (2.5°N to 2.5°S) sea surface temperatures in the Pacific and Indian Oceans from years 1 to 30 of the model integration. The contours are every 1°C, stippling is used for temperatures greater than 27°C and cross hatching for temperatures greater than 29°C. Below 27°C every alternate contour is dashed. The minimum yearly temperature in the east Pacific is shown.

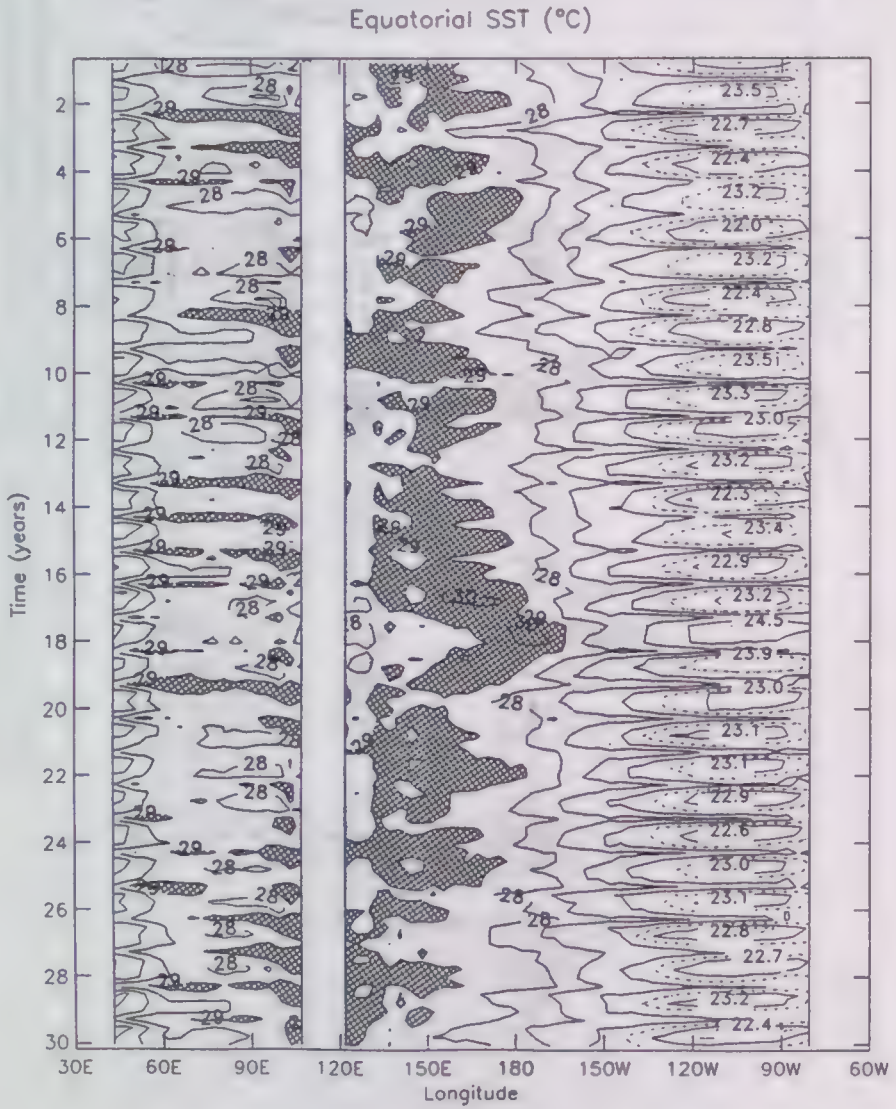

Figure 10: Observed time/longitude plot of sea surface temperatures
This plot shows a time/longitude plot for the equatorial sea surface temperatures from the 30 year period 1960 to 1990. The contour interval and shading are the same as that in Fig. 9.

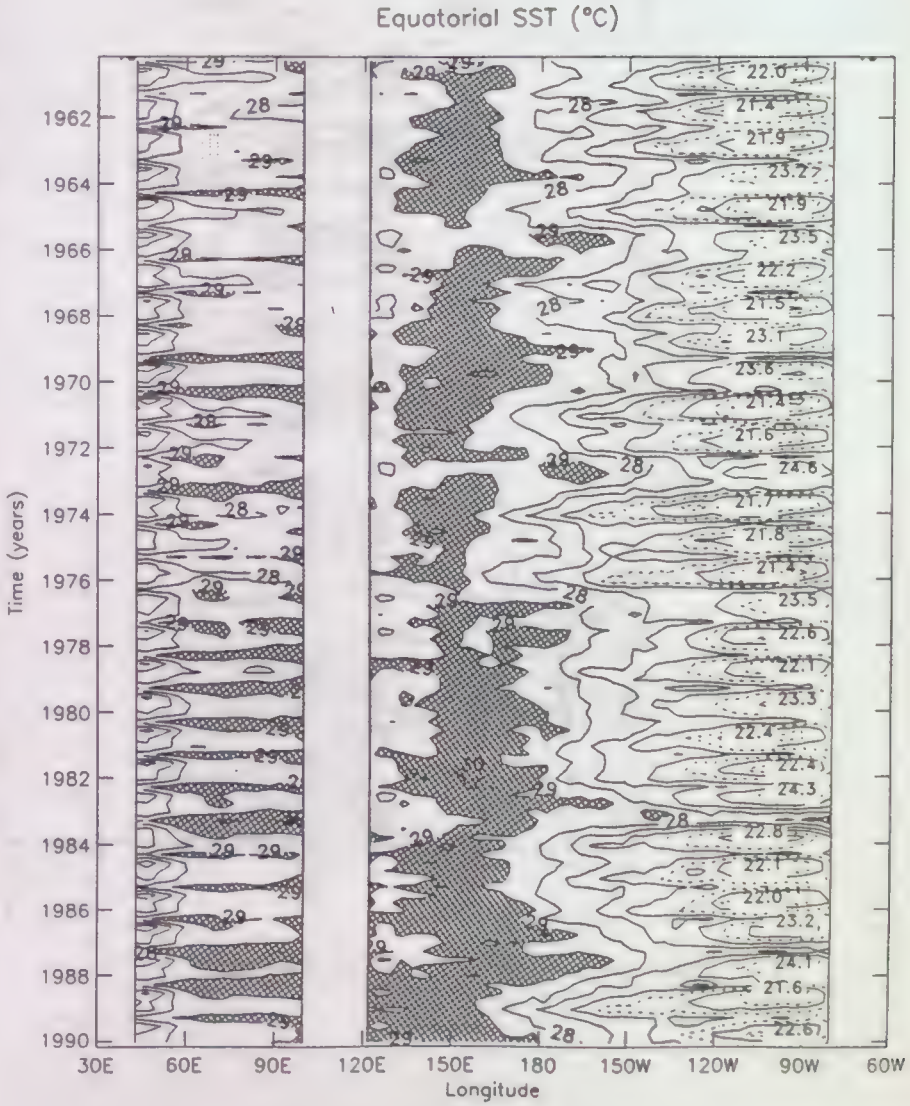

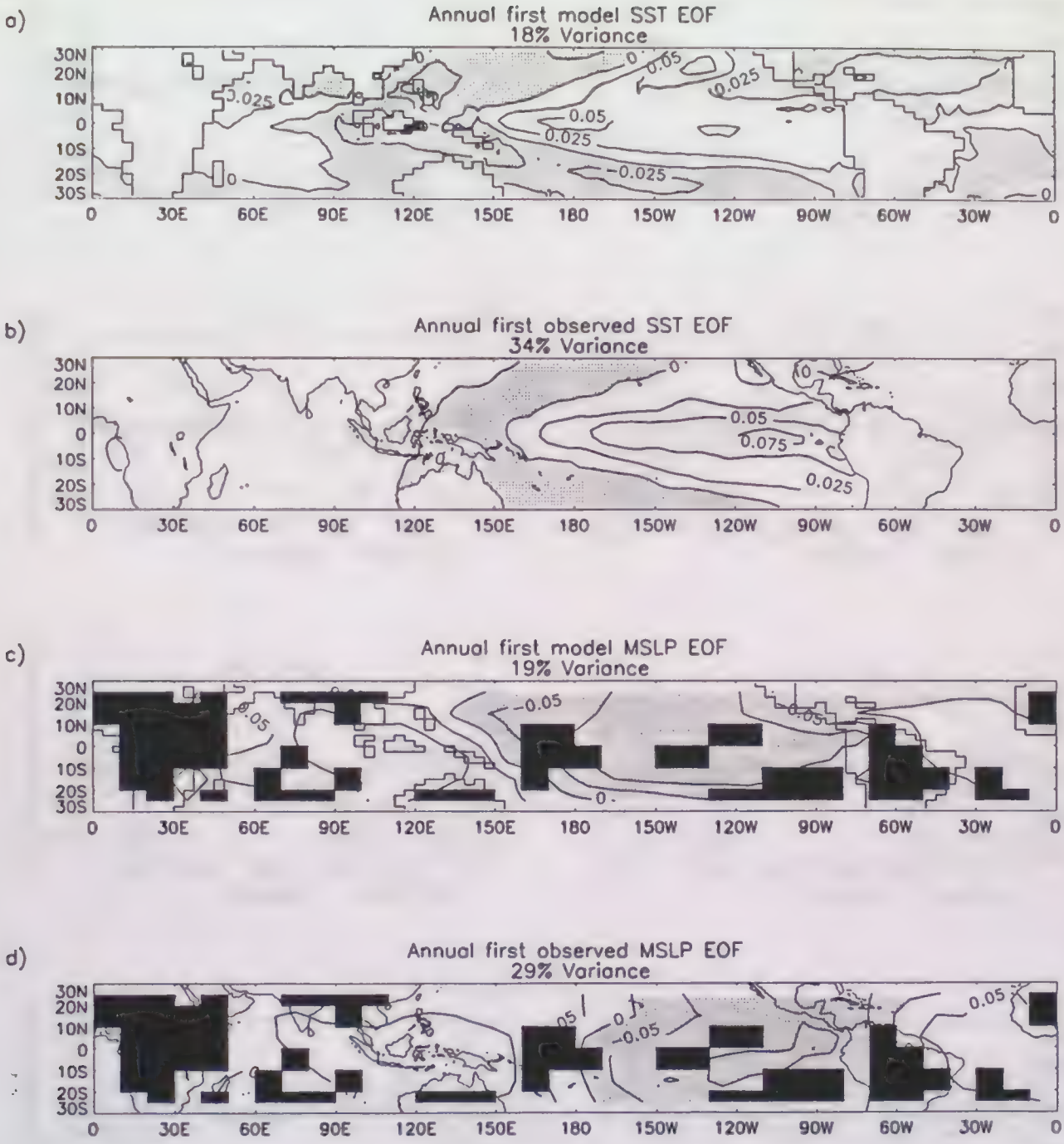

Figure 11: Model and observed EOFs

Figures (a) and (b) are plots of the first model and observed EOFs, of the correlation matrix, using sea surface temperature data with the seasonal cycle removed. The contour interval is 0.025 with stippling for negative anomalies. Both EOFs are orthonormalized such that they have positive weights in the east Pacific.

Figures (c) and (d) show the first model and observed EOFs for the mean sea level pressure. The contour interval is 0.05 with stippling for negative values. Both EOFs have been orthonormalized such that they have positive weights in the Indonesian region.

In all the plots the fraction of the total variance explained by each EOF is shown.

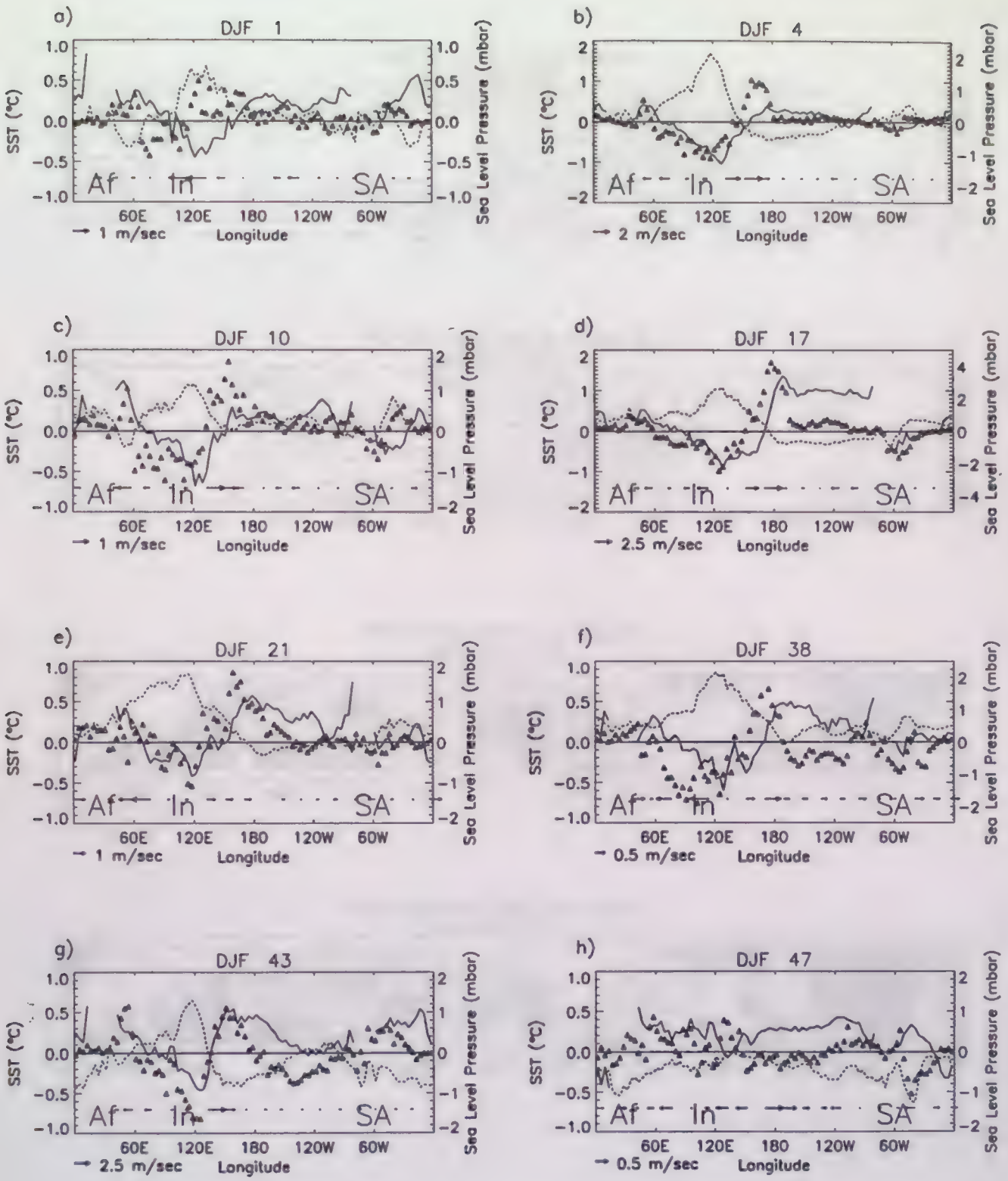

Figure 12: Model warm event meridional means

Figures (a)–(h) show meridional means, for the region 10°N to 10°S, of sea surface temperatures, sea level pressure, precipitation and the eastwards components of surface wind during DJF for the eight model warm events. All values are anomalies relative to the 50 year climatology.

In all plots the SST is shown as a solid line, pressure as as dashed line, precipitation as small triangles and the wind anomalies as arrows, positive (eastwards) anomalies being directed to the right. For the wind anomalies a scaling arrow is shown in the bottom lefthand corner of each plot. The SST anomalies use the lefthand scale on the plot while the pressure anomalies use the righthand scale. All precipitation anomalies are in mm/day, have been scaled by 0.2 and use the lefthand SST scale. In all plots approximate positions of Africa, Indonesia and South America are shown by Af, In and SA respectively.

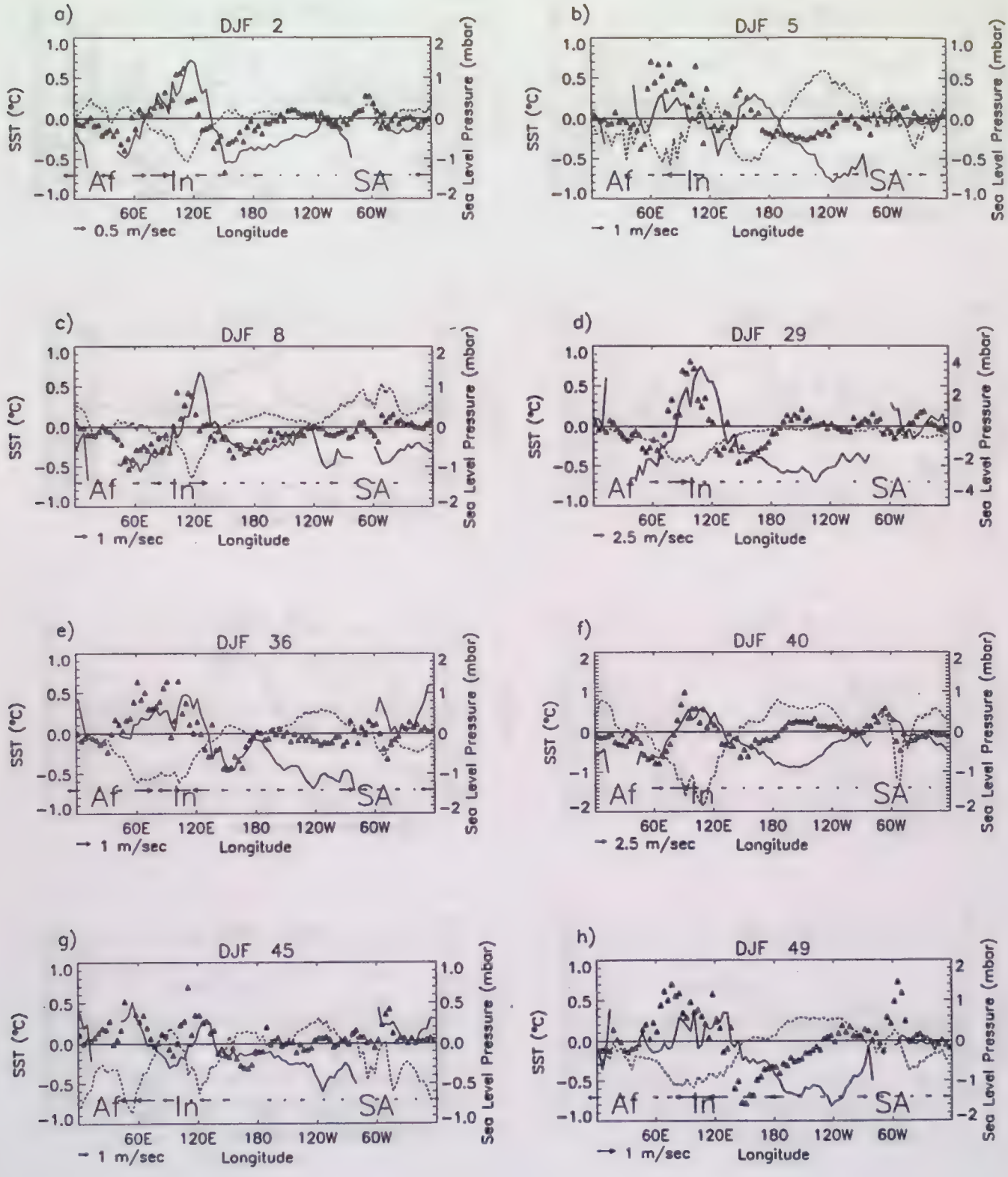

Figure 13: Model cold event meridional means

Figures (a)-(h) show meridional means, for the region 10°N to 10°S, of sea surface temperatures, sea level pressure, precipitation and the eastwards components of wind during DJF of the eight model cold events. All values are anomalies relative to the 50 year climatology. The explanation of the plots is the same as for Fig. 12.

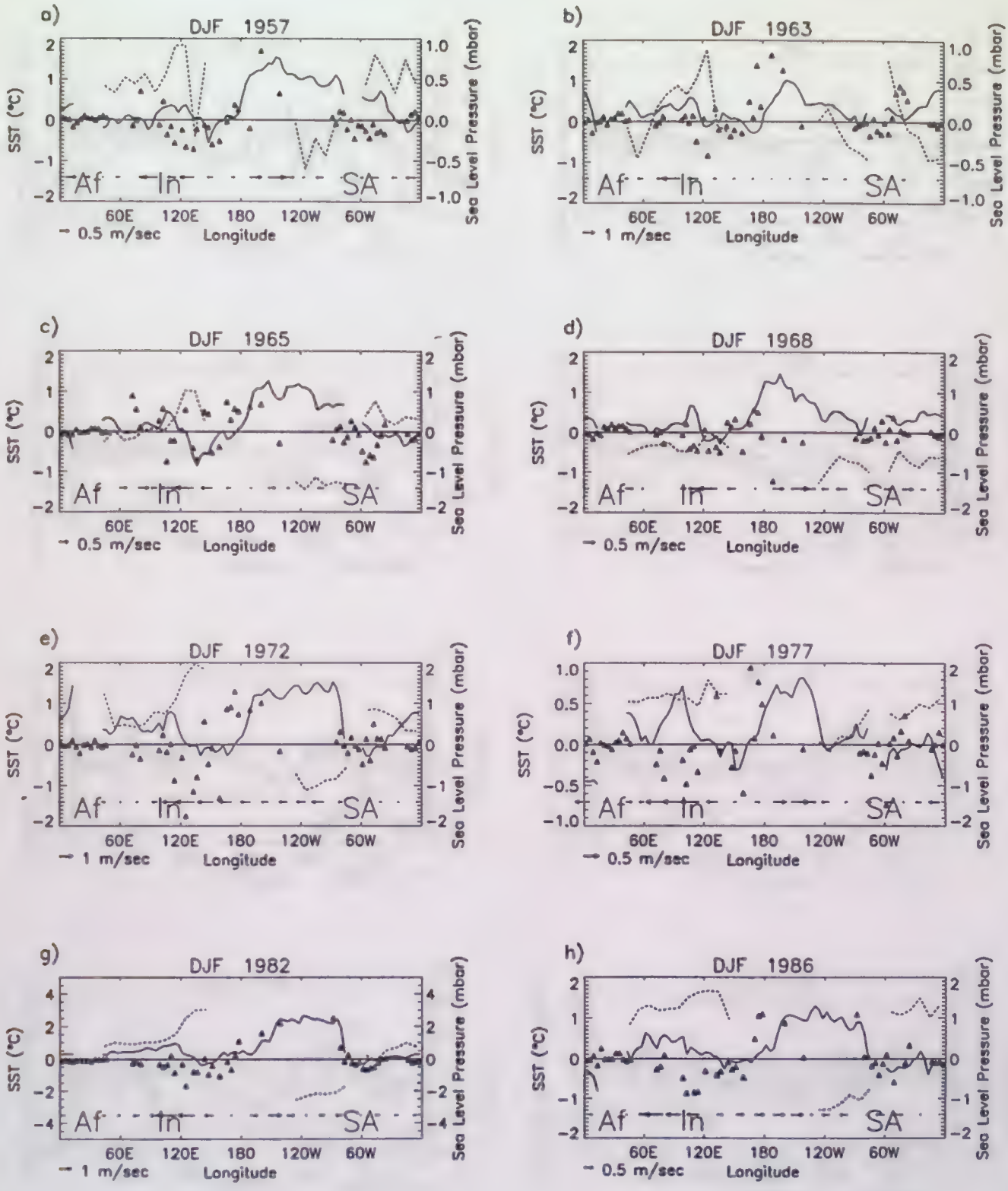

Figure 14: Observed warm event meridional means

Figures (a)–(h) show meridional means, for the region 10°N to 10°S, of sea surface temperatures, sea level pressure, land station precipitation and the eastwards components of wind during DJF of the eight observed warm events since 1957. All values are anomalies relative to the climatology from the period 1948 to 1990. The explanation of the plots is the same as that for Fig. 12.

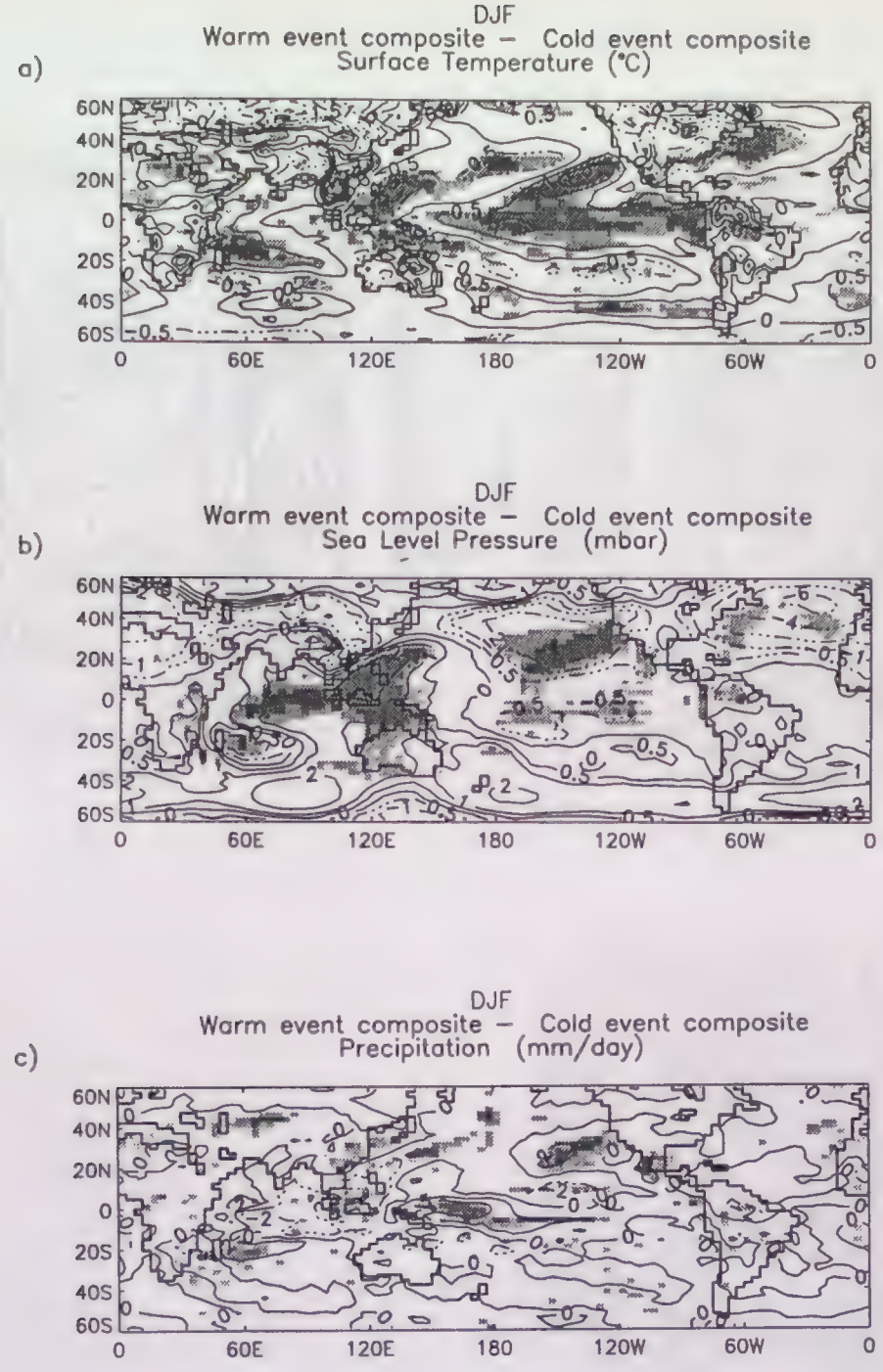

Figure 15: Composite warm - composite cold for DJF

Plot (a): temperature difference between composite warm event DJF and composite cold DJF event. The contour interval is 0.5°C. Plot (b): pressure difference with contours at $0.0, \pm 0.5, \pm 1.0, \pm 2.0$ mbar and then with a separation of 2.0 mbar thereafter. Plot (c): precipitation difference with a contours at $0, \pm 2 \pm 5$ mm/day and then with a separation of 5 mm/day thereafter.

In all plots regions of significant differences, at the 5% level, are shown as light shading while regions where the differences are significant at the 1% level are shown with darker shading. Negative contours are shown as dot dashed lines.

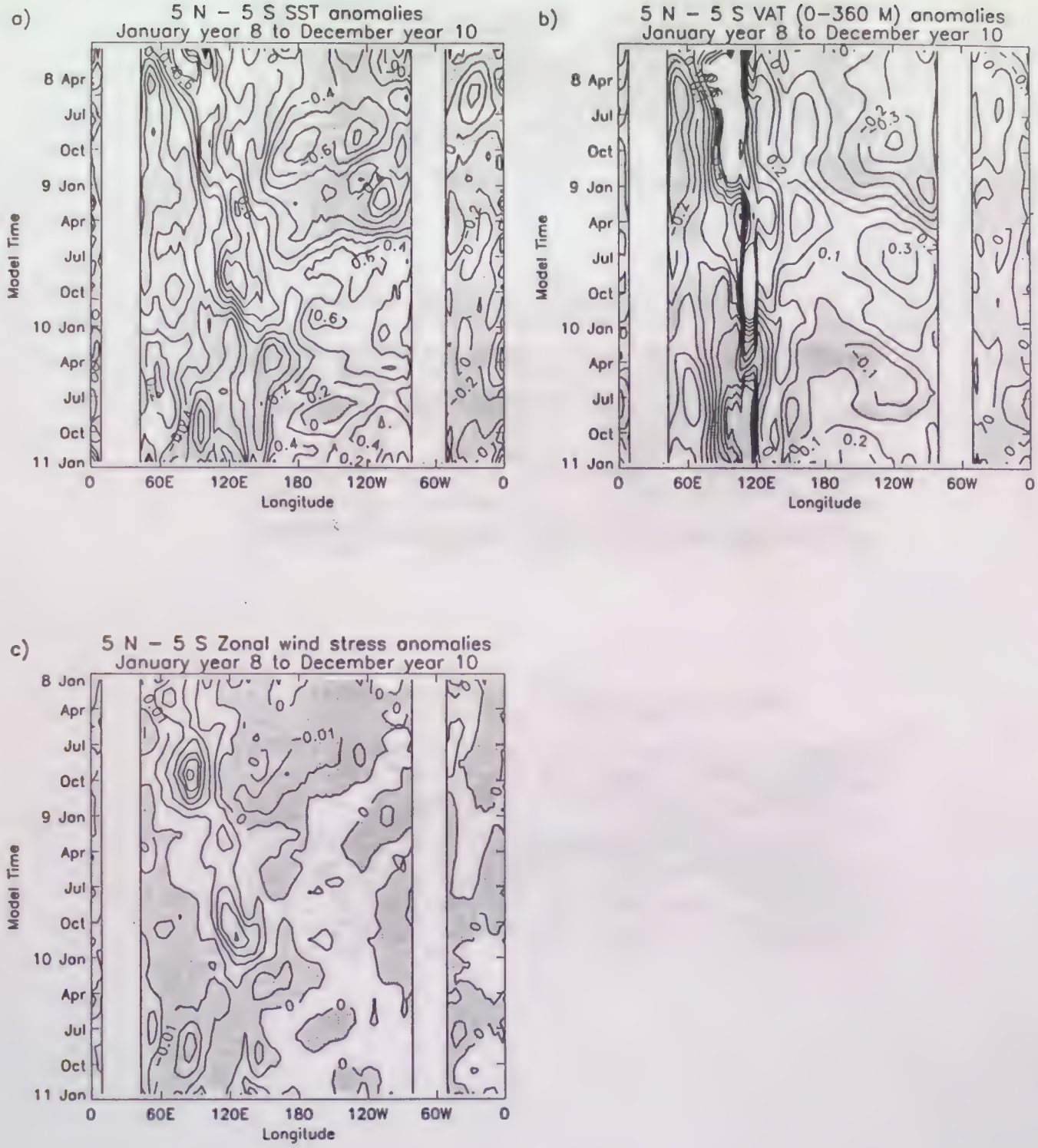

Figure 16: Time/longitude plots for year 10 warm event

Plot (a) shows SST anomalies with a contour interval of 0.2° C. Stippling has been used for negative anomalies. The data were smoothed using a 1-2-1 smoother in each direction prior to plotting.

Plot (b) shows VAT anomalies with a contour interval of 0.1° C. Negative anomalies are stippled.

Plot (c) shows anomalous zonal wind stress using a contour interval of 0.01 N/m^2. Easterly anomalies are shown stippled. The data were smoothed using a 1-2-1 smoother in each direction prior to plotting.

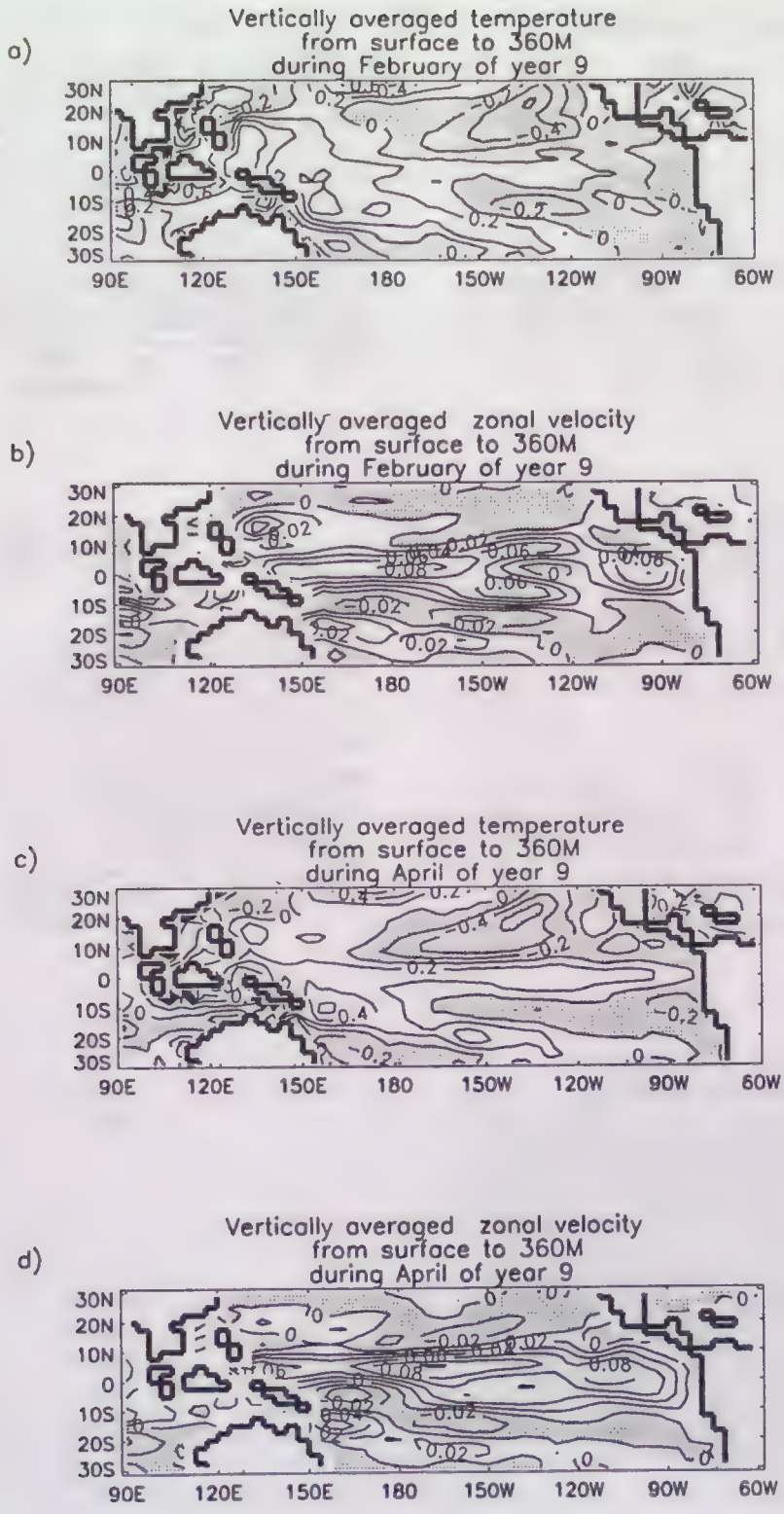

Figure 17: Vertically averaged temperature and zonal velocity
Plots (a) and (c) are of the vertically averaged temperature anomalies for February and April during year 9. A contour interval of 0.2°C is used. Plots (b) and (d) show the vertically averaged zonal velocity anomalies during the same period. A contour interval of 0.02m/sec is used. In both plots negative anomalies are shown stippled.

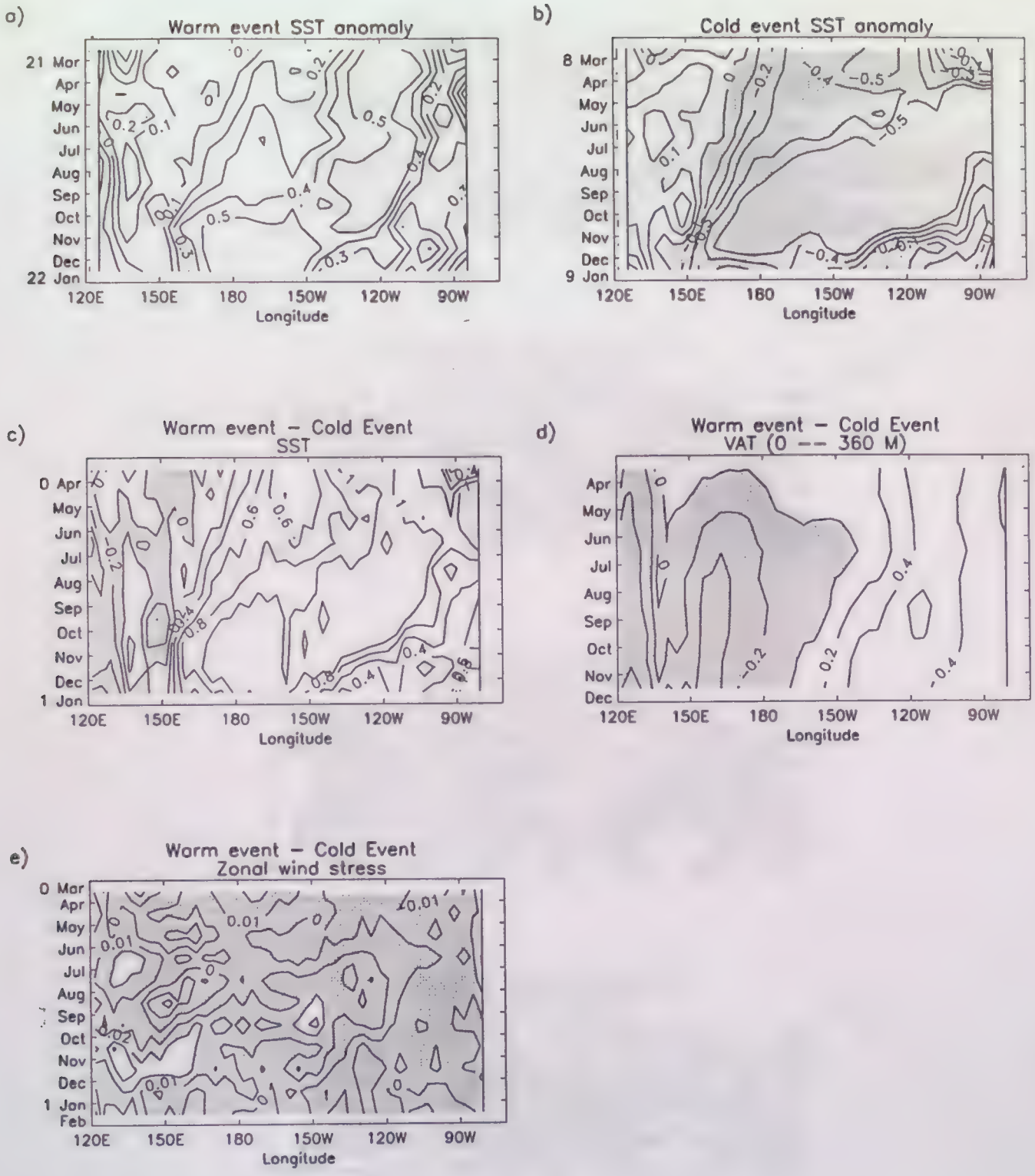

Figure 18: Warm event − cold event differences

All plots are time-longitude plots for the equatorial Pacific (10°N to 10°S) and were smoothed using a 1-2-1 smoother in each direction prior to plotting. In all plots negative values are stippled.

Plots (a) and (b) are of SST anomalies for the warm event of year 21 and the cold event of year 8. They both have contours at −0.75°C and and 0.75°C and from −0.6°C to 0.6°C they use a contour interval of 0.1°C.

Plots (c), (d) and (e) show differences for SST, vertically averaged temperature to a depth of 360 metres and zonal wind stress between the warm event and cold event. Plots (c) and (d) both have contours at −1.5° and 1 − 5°C and then use a contour interval of 0.2°C from −1.2°C to 1.2°C. Plot (e) uses a contour interval of 4×10^{-3} N/m^2.

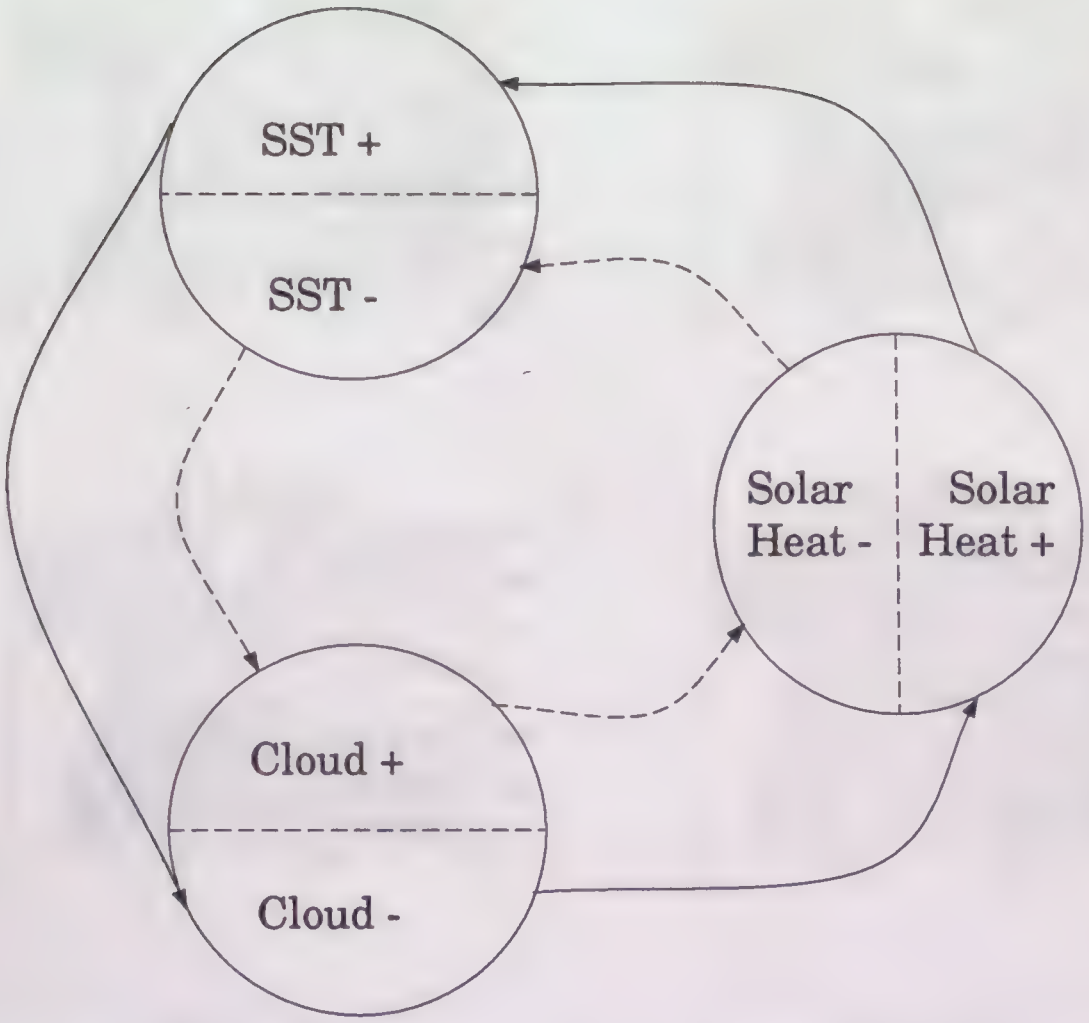

Figure 19: Schematic Cloud, SST feedback
The feedback loop is shown by arrows: dashed for a possible cooling feedback, solid for a possible warming feedback. The processes in the loop are shown in the circles connected by the arrows.

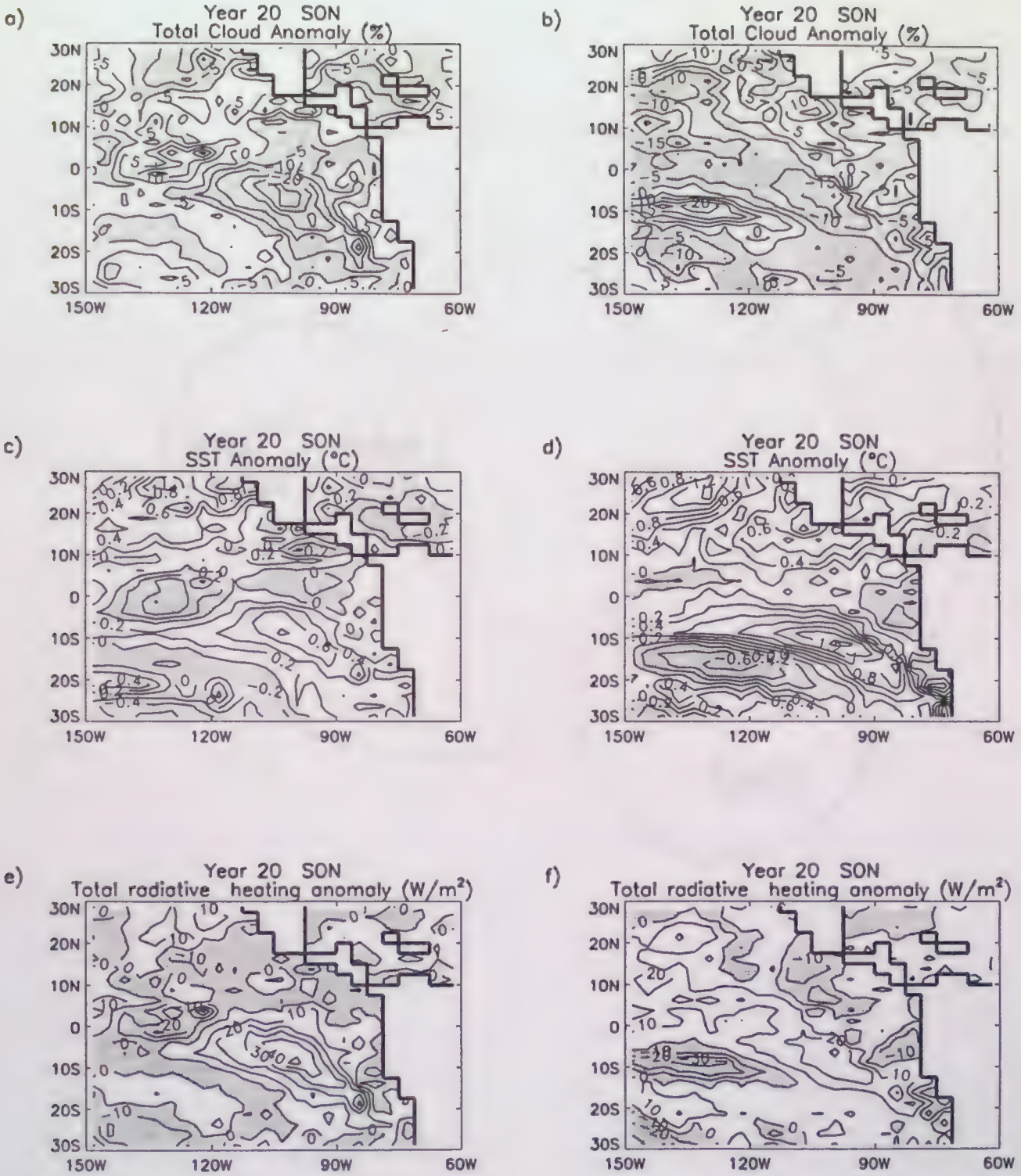

Figure 20: SST, cloud and radiative heating

In all plots stippling denotes negative anomalies.

Plots (a) and (b) show the total cloud seasonal anomalies in the eastern Pacific with a contour interval of 5% for SON and DJF of year 20 respectively. Plots (c) and (d) show the SST seasonal anomalies for the same region and times using a contour interval of 0.2°C. Plots (e) and (f) show the total radiative heating anomalies for the same region and times with a contour interval of $10 W/m^2$ is used.

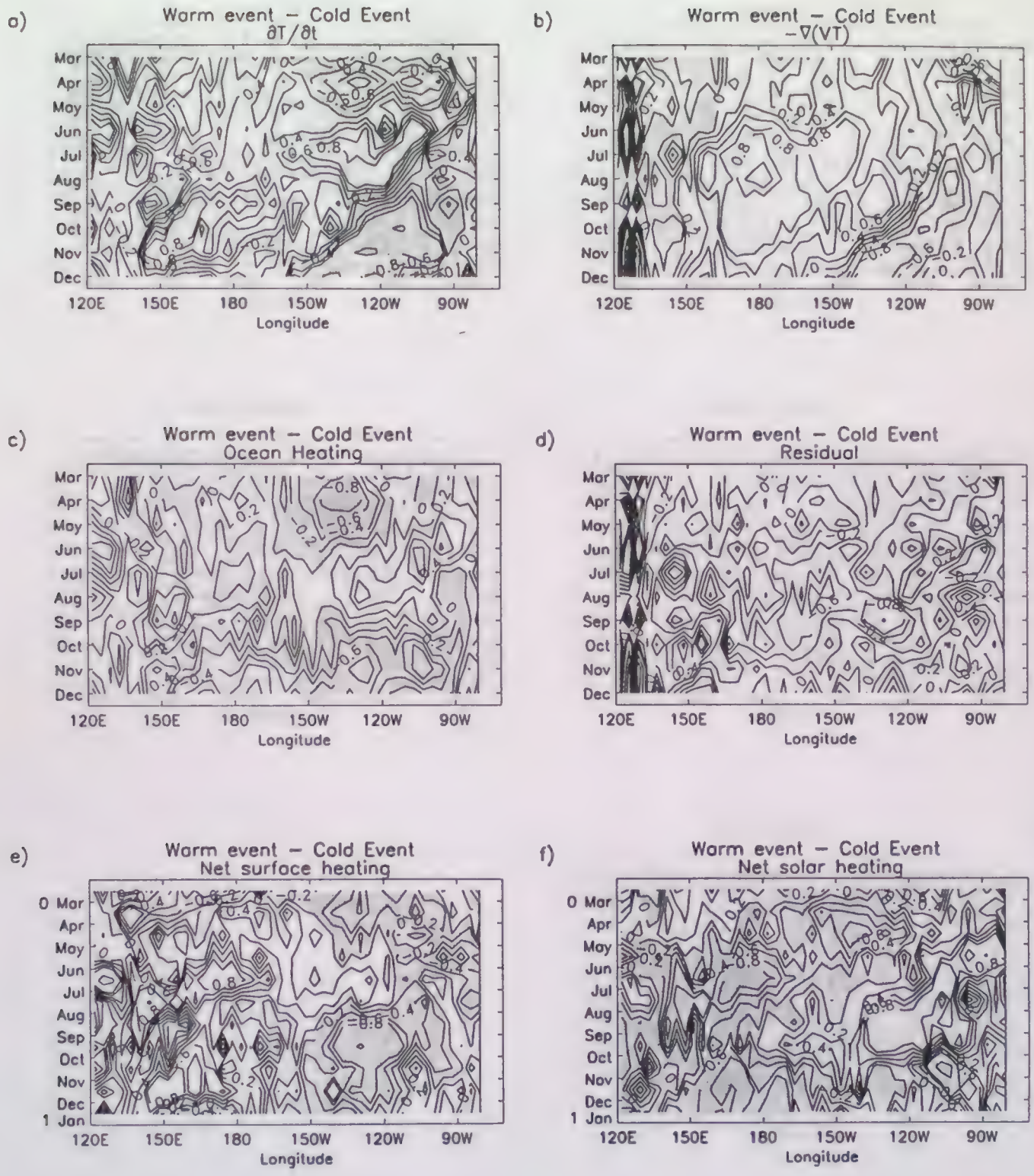

Figure 21: Warm - cold event heat budget

All plots are time-latitude plots for the equatorial Pacific region between 10°N and 10°S to a depth of 55.5 metres, have had a 1-2-1 smoother applied in both directions and stippling is used for negative anomalies.

Plot (a) shows the difference in the temperature change between the warm and the cold event. Plots (b), (c) and (d) show the contributions to the total temperature change from advection, ocean heating and the residual. Plots (e) and (f) show the contributions to ocean heating from heating through the surface and from solar heating respectively. Plots (g) and (h) show the contributions to the advective heating from the mean velocity acting on temperature differences and the velocity difference acting on the mean temperature respectively. In plots (a) to (h) a contour interval of 0.2°C/100 days is used.

The zonal, meridional and vertical contributions to plot (h) are shown in plots (i), (j) and (k) with a contour interval of 1.0°C/100 days.

Figure 21: Continued

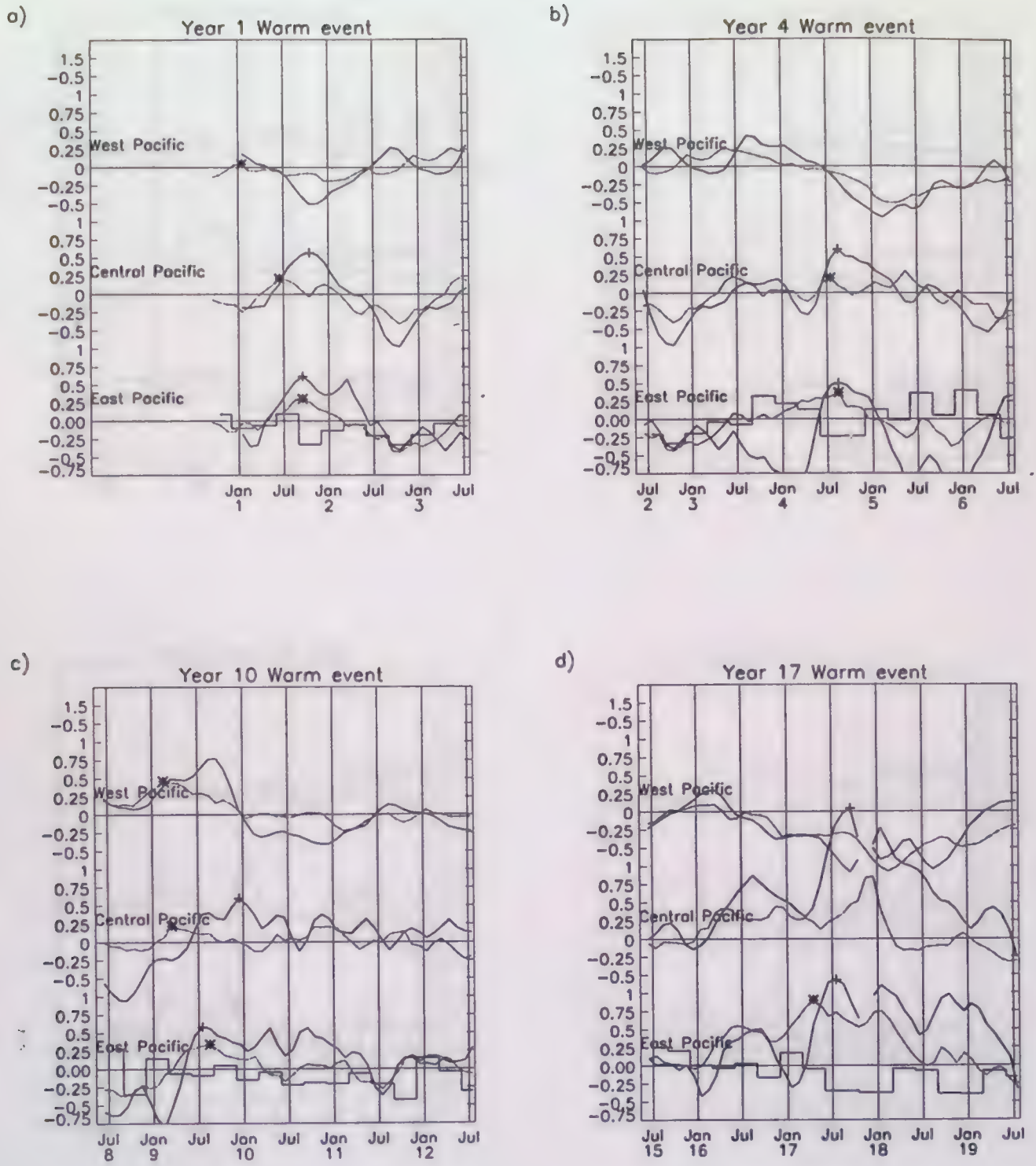

Figure 22: VAT, SST and layer cloud for all model warm events

Plots (a)-(h) show time series of SST, VAT and low level cloud anomalies for 18 months prior to the year of an event, the year of the event, and the 18 months after the year of the event. Each plot shows area averages of VAT and SST anomalies for three regions: east Pacific (120°W to 90°W); central Pacific (180° to 150°W); west Pacific (120°E to 150°E). All regions are from 10°N to 10°S. Area averaged low level cloud anomalies for a region with maximum mean cloud (0° to 10°S and 120°W to 100°W) in the east Pacific are also shown.

Area averaged values of VAT anomalies are shown with dot dashed lines, SST anomalies as a solid line and cloud anomalies with a histogram. Positions of the maximum values, associated with a model ENSO, of VAT and SST have also been shown on the plots as asterisks for the VAT plots and crosses for the SST plots. The cloud values were scaled by a factor of 4 prior to plotting.

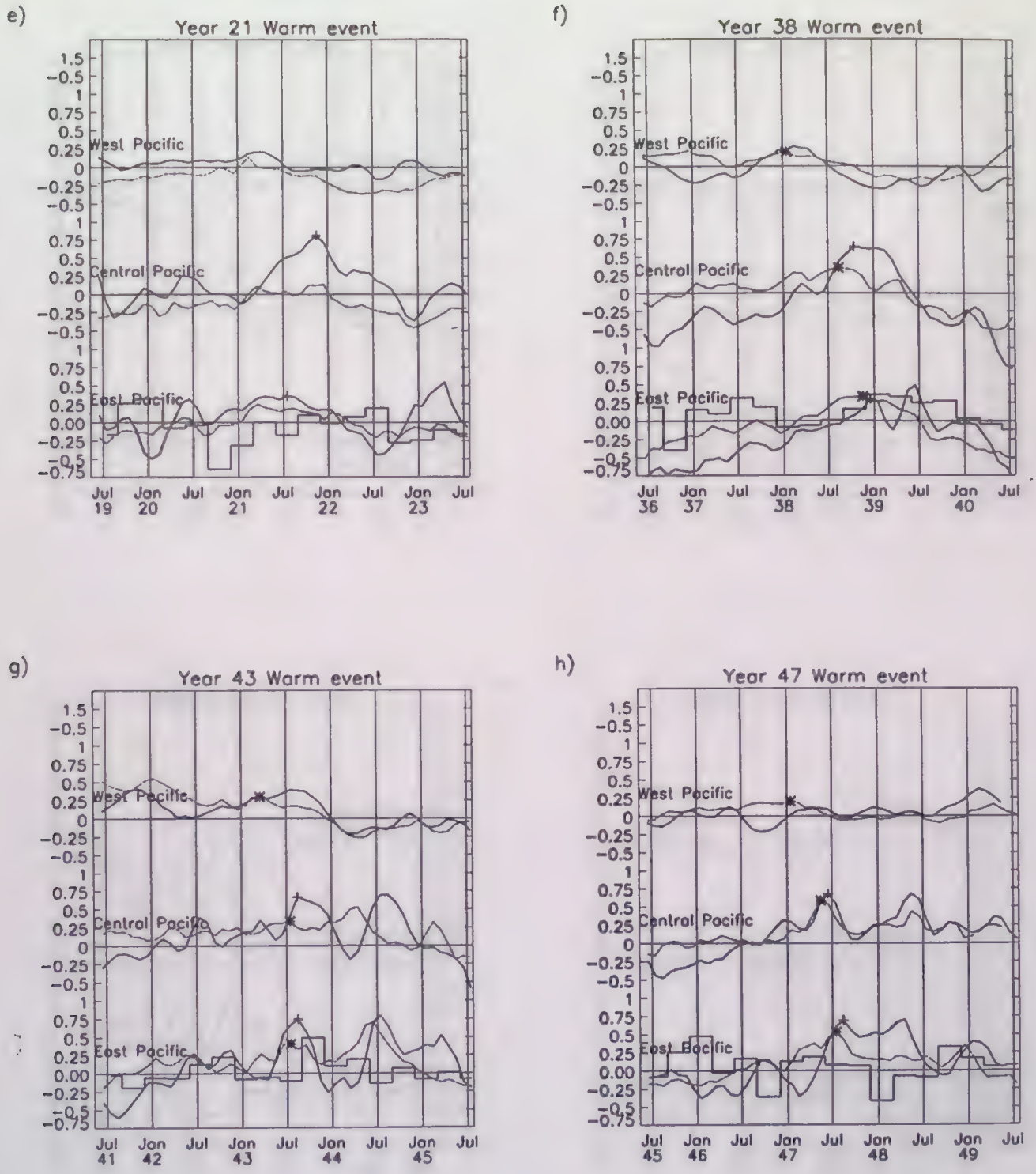

Figure 22: Continued

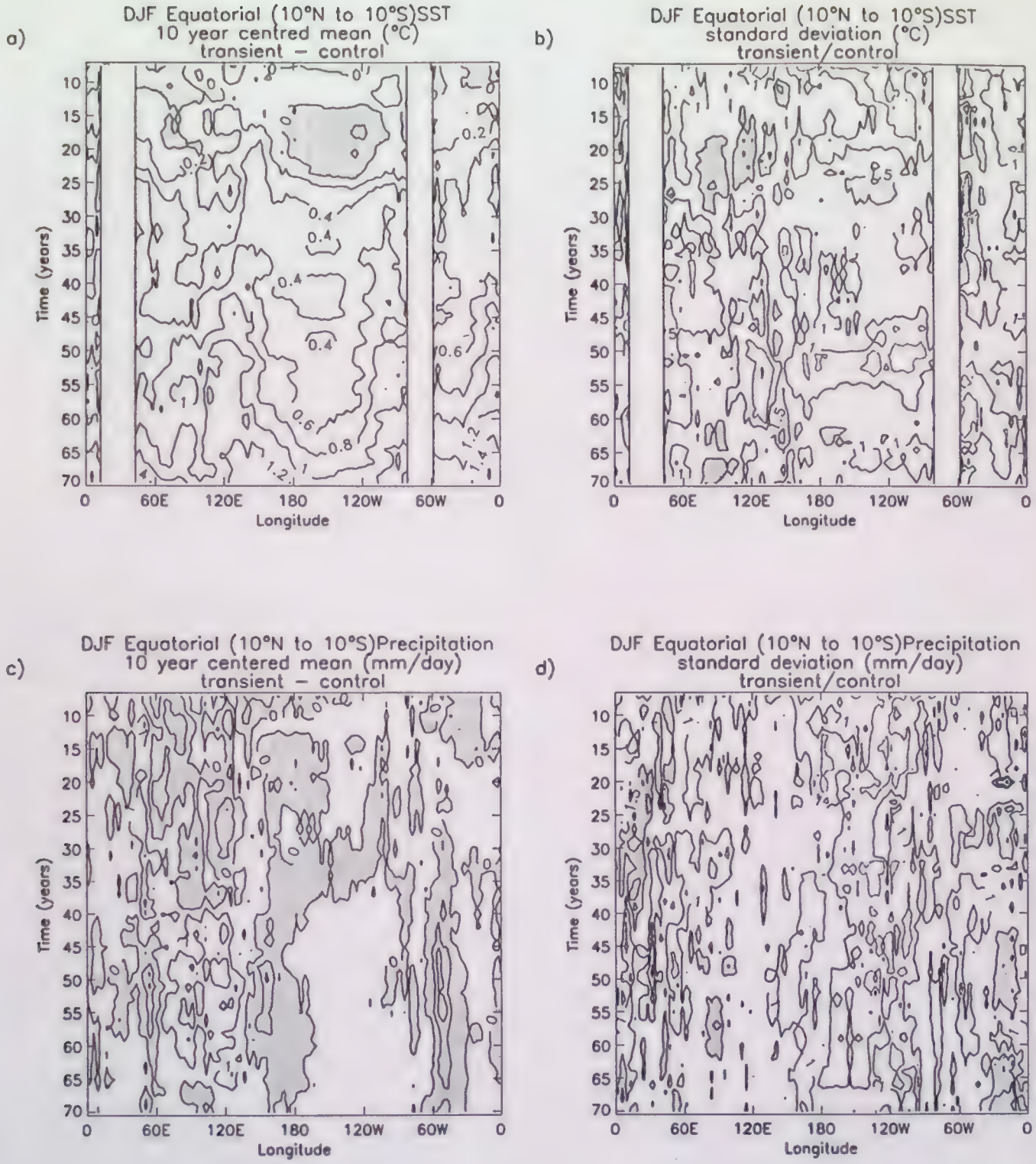

Figure 23: Interannual Variance and 10 year running means

Plots (a) and (c) show time-longitude cross sections of the 11 year centred mean differences between the transient and the control experiments for the SST and precipitation respectively. Plots (b) and (d) show the standard deviations computed in 11 year periods for the transient experiment divided by the standard deviation from the equivalent period for the control experiment for the SST and precipitation respectively.

In (a) a contour interval of 0.2°C is used. A contour interval of 1.0mm/day is used in (c). In both plots (a) and (c) stippling is used for negative differences. In both of plots (b) and (d) contours are drawn at values of 0.0, 0.25, 0.5, 0.75, 1.0, 1.5 and 2.0 with stippling for values greater than 1.5. Contour lines for values less than one are shown with dashed lines in the plots of standard deviation ratios.

CLIMATE RESEARCH TECHNICAL NOTES

CRTN 1	Oct 1990	Estimates of the sensitivity of climate to vegetation changes using the Penman-Monteith equation. P R Rowntree
CRTN 2	Oct 1990	An ocean general circulation model of the Indian Ocean for hindcasting studies. D J Carrington
CRTN 3	Oct 1990	Simulation of the tropical diurnal cycle in a climate model. D P Rowell
CRTN 4	Oct 1990	Low frequency variability of the oceans. C K Folland, A Colman, D E Parker and A Bevan
CRTN 5	Dec 1990	A comparison of 11-level General Circulation Model Simulations with observations in the East Sahel. K Maskell
CRTN 6	Dec 1990	Climate Change Prediction. J F B Mitchell and Qing-cun Zeng
CRTN 7	Jan 1991	Deforestation of Amazonia - modelling the effects of albedo change. M F Mylne and P R Rowntree
CRTN 8	Jan 1991	The role of observations in climate prediction and research. D J Carson
CRTN 9	Mar 1991	The greenhouse effect and its likely consequences for climate change. D J Carson
CRTN 10	Apr 1991	Use of wind stresses from operational N.W.P. models to force an O.G.C.M. of the Indian Ocean. D J Carrington
CRTN 11	Jun 1991	A new daily Central England Temperature series, 1772-1991. D E Parker, T P Legg and C K Folland
CRTN 12	Jul 1991	Causes and predictability of Sahel rainfall variability. D P Rowell, C K Folland, K Maskell, J A Owen, M N Ward

CLIMATE RESEARCH TECHNICAL NOTES

CRTN 13	Jul 1991	Modelling changes in climate due to enhanced CO2, the role of atmospheric dynamics, cloud and moisture. C A Senior, J F B Mitchell, H Le Treut and Z-X Li
CRTN 14	Sep 1991	Sea temperature bucket models used to correct historical SST data in the Meteorological Office. C K Folland
CRTN 15	Aug 1991	Modelling climate change, and some potential effects on agriculture in the U.K. P R Rowntree, B A Callander and J Cochrane
CRTN 16	Aug 1991	The Boreal Forests and Climate G Thomas and P R Rowntree
CRTN 17	Aug 1991	Development of a Stratosphere-Troposphere Data Assimilation System. R Swinbank.
CRTN 18	Sep 1991	A study of asynchronous coupling using a simple climate model. M K Davey.
CRTN 19	Sep 1991	The Oceanic Carbon Cycle. N K Taylor
CRTN 20	Nov 1991	Worldwide ocean-atmosphere surface fields in Sahel wet and dry years using provisionally corrected surface wind data. M N Ward
CRTN 21	Dec 1991	Coupled tropical ocean global atmosphere models at the UKMO. M K Davey, C Gordon, S Ineson and S Lawrence
CRTN 22	Dec 1991	Empirical parameterisation of tropical ocean-atmosphere coupling. M Allen, M K Davey, D L T Anderson and P D Killworth
CRTN 23	Feb 1992	The temporal evolution of Equatorial Currents in the Indian Ocean D L T Anderson, D J Carrington, R A Corry and C Gordon
CRTN 24	Feb 1992	Stratospheric analyses provided by the U.K. Meteorological Office M J Bailey, A O'Neill and V D Pope

CLIMATE RESEARCH TECHNICAL NOTES

CRTN 25	Feb 1992	Modelling interannual variability in the Indian Ocean using momentum fluxes from the UKMO and ECMWF operational weather analyses. D L T Anderson and D J Carrington
CRTN 26	Mar 1992	A GCM simulation of the impact of Amazonian deforestation on climate using an improved canopy representation J Lean and P R Rowntree
CRTN 27	Mar 1992	The parameterization of rainfall interception in GCMs A J Dolman and D Gregory
CRTN 28	Jun 1992	Development of worldwide marine data eigenvectors since 1985 A W Colman
CRTN 29	Jun 1992	A tropical ocean model with reduced physics M K Davey
CRTN 30	Jun 1992	International Temperature Workshop, Boulder, Colorado, USA, 16 January 1992 Edited by D E Parker
CRTN 31	Jul 1992	Simulation of clear-sky outgoing longwave radiation over the oceans using operational analyses A Slingo and M J Webb
CRTN 32	Sep 1992	A prediction of the transient response of climate J M Murphy
CRTN 33	Nov 1992	LEPS scores for assessing climate model simulations and long-range forecasts. C K Folland
CRTN 34	Jan 1993	Stratospheric Data Assimilation System Guide Editer: R Swinbank
CRTN 35	Mar 1993	A Stratosphere-Troposphere Data Assimilation System R Swinbank and A O'Neill
CRTN 36	Mar 1993	Validation of hydrological schemes for climate models against catchment data. P R Rowntree and J Lean

CLIMATE RESEARCH TECHNICAL NOTES

CRTN 37	Apr 1993	Modelling of palaeoclimates: Examples from the recent past J F B Mitchell
CRTN 38	May 1993	A simulation of seasonality in ENSO forecast skill M K Davey, D L T Anderson and S Lawrence
CRTN 39	Jul 1993	ENSO Prediction experiments using a simple ocean-atmosphere model D-H Wu, D L T Anderson and M K Davey
CRTN 40	Sep 1993	Diagnosis of dynamic sea-surface and sea-level changes from the Cox ocean model J M Gregory
CRTN 41	Sep 1993	Seasonal variations of the clear-sky greenhouse effect: the role of changes in atmospheric temperatures and humidities M J Webb, A Slingo and G L Stephens
CRTN 42	Nov 1993	Sea-level changes under increasing atmospheric CO_2 in a transient coupled ocean-atmosphere GCM experiment. J M Gregory
CRTN 43	Dec 1993	Global and regional patterns of climate change: recent predictions for the Arctic P R Rowntree
CRTN 44	Feb 1994	The effect of changing horizontal diffusion in the atmospheric version of the unified climate model C D Hall and R A Stratton
CRTN 45	Mar 1994	Simulation of El-Niño/Southern Oscillation like variability in a global AOGCM and its response to CO_2 increase. S F B Tett